Coastal warming off Tokai during the Kuroshio large meander period revealed by SST and SSH data

XU, JIAKE
九州大学総合理工学府大気海洋環境システム学専攻

出版情報：Kyushu University, 2022, 修士, 修士
バージョン：
権利関係：

Coastal warming off Tokai during the Kuroshio large meander period revealed by SST and SSH data

JIAKE XU

Supervisor: Kaoru Ichikawa

Interdisciplinary Graduate School of Engineering Sciences

Kyushu University

Contents

1. Introduction

The Kuroshio is a western boundary current, which carries amounts of heat and salt from the tropic region to the mid-latitude region of the western north pacific. When it comes to the dynamic characteristics of Kuroshio current, the surface velocity of Kuroshio current can reach up to 2.0-2.5 m /s.

Seeing from the flow of the Kuroshio, the sea surface height difference between the offshore side and the shore side can reach up to 1 m (the sea surface height near the Kuroshio is higher on the right side than on the left side). Since the Kuroshio current is approximately regarded as the current with geostrophic balance, the sea surface height difference can be explained by the geostrophic balance theory. Furthermore, the velocity of Kuroshio current is strongly related with the depth. It decreases with depth, which can always extend to around 1000 m.

Kuroshio current can be regarded as a complicated system. There are several parts of the Kuroshio Current System: the upstream Kuroshio in the area east of Taiwan, the Kuroshio near the East China Sea (ECS), the Kuroshio between the Tokara Strait and the Izu-Ogasawara Ridge, and the Kuroshio Extension (KE) east of Japan.

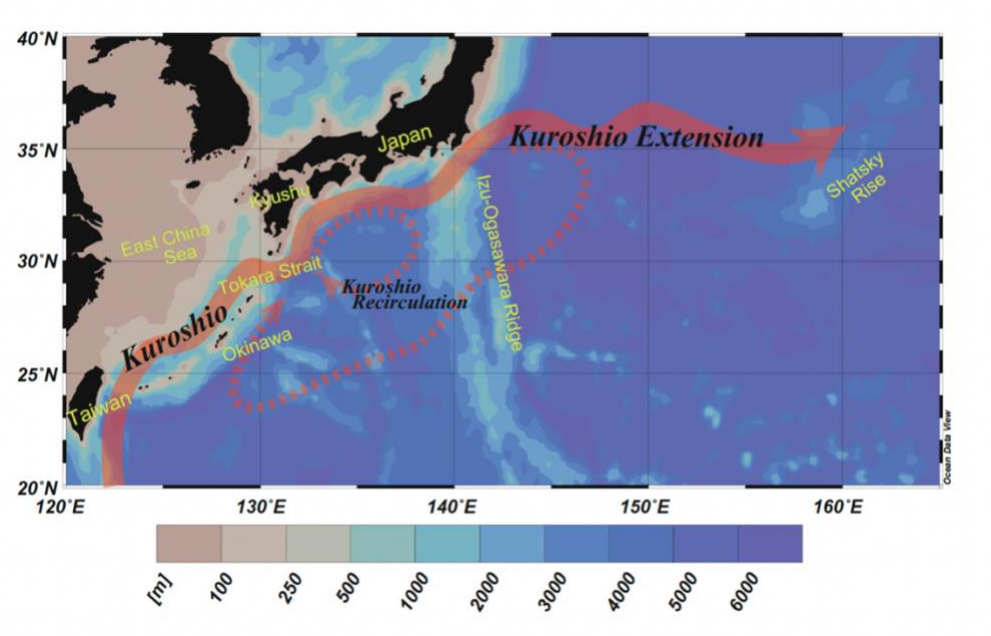

Figure.1.1 Schematic map of the Kuroshio Current System with bathymetry contours, from Ichikawa (2019)

For the Kuroshio current off south coast of Japan, it has two typical paths with bimodal feature: large meander (LM) path and non-large-meander (NLM) path, which has been well defined by previous study (Kawabe,1985). Both two paths usually remain for several years, which are relatively stable.

The NLM path can be further divided into two paths: the offshore NLM (oNLM) path and nearshore NLM (nNLM) path (Kawabe, 1995). Some researchers suggest that characteristics of these paths are related to the ocean bottom topography south of Honshu.

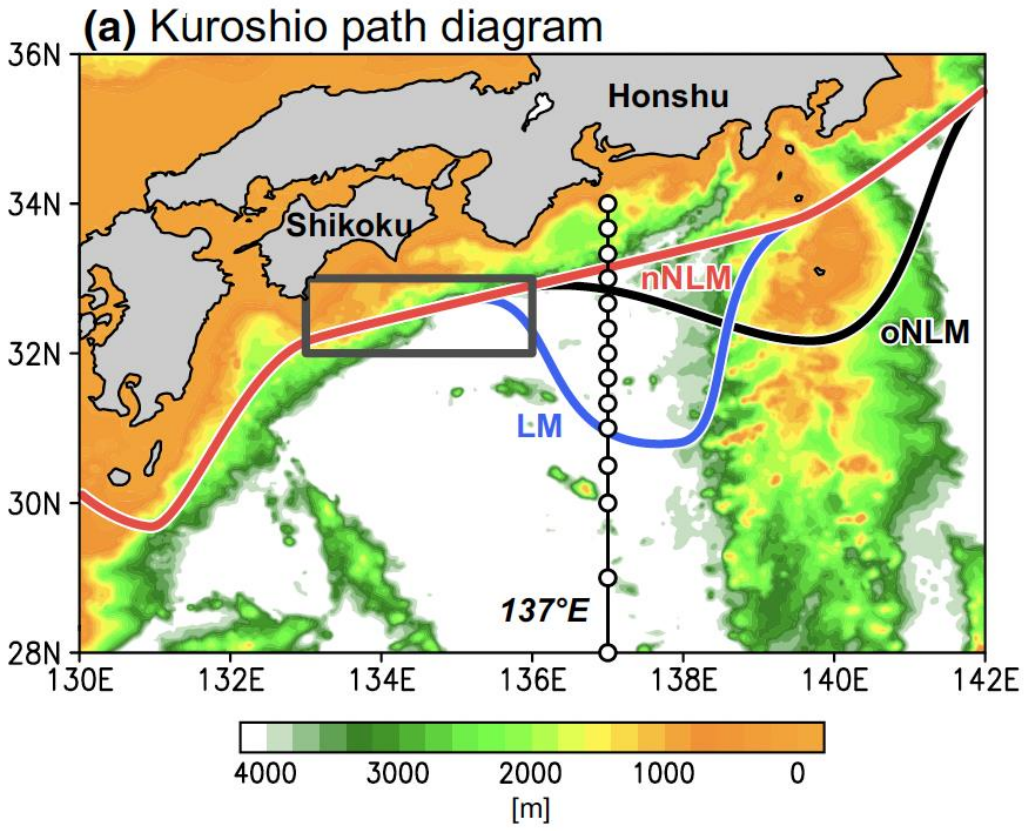

Figure.1.2 Three typical paths of the Kuroshio south of Japan, from Sugimoto et al. (2019)

As shown in Table.1.1, Kuroshio LM phenomenon usually existed for more than one year. The most recent Kuroshio LM event happened since the summer of 2017, and the interesting thing is that it has become the longest LM period in the LM observation history.

LM period	Duration
1. August 2017 ~	4 years and 9 months (until April 2022)
2. August 1975 ~ March 1980	4 years and 8 months
3. November 1981 ~ May 1984	2 years and 7 months
4. December 1986 ~ July 1988	1 year and 8 months
5. July 2004 ~ August 2005	1 year and 2 months
6. December 1989 ~ December 1990	1 year and 1 month

Table.1.1 Kuroshio Large meander after 1965 (List from the longer duration to shorter duration)

For the area between the shore region and the southern coast of Tokai district, a strong cyclonic eddy has been well distinguished during LM periods by satellite data. The large cool water pool can extend to several kilometers and the characteristic of water is like the water of Kuroshio current. It has been considered that the deep layer water of the Kuroshio upwelled ,thus caused the LM-induced cool water pool.
In Figure.1.3, mean sea surface temperature from 2017.09 to 2019.04 is calculated, based on Himawari SST dataset.The fishering and climate off Tokai district can be well influenced by this cool water pool.

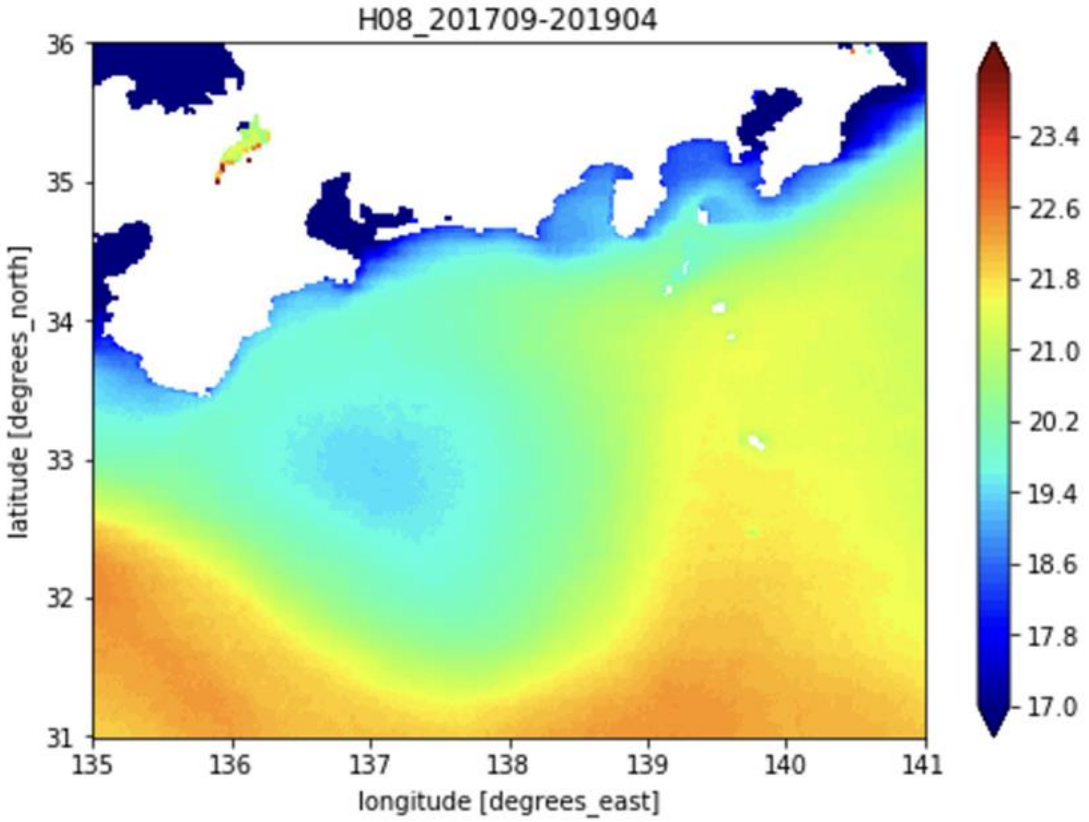

Figure.1.3　Mean SST(°C) during LM period (2017.09-2019.04)

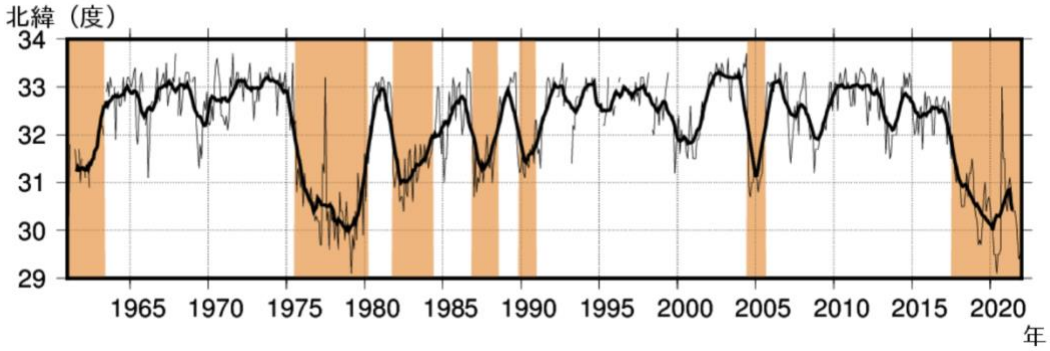

Figure.1.4　Variation of the southernmost latitude of the Kuroshio path off the Tokai district (January 1961-December 2021)

(From JMA, https://www.data.jma.go.jp/kaiyou/data/shindan/b_2/kuroshio_stream/kuroshio_stream.html)

It is commonly recognized that the variation of Kuroshio's path can affect the sea level for time scales longer than a few months. For smaller time scales, tides, winds, and atmospheric pressure play a leading role (Zhang, Ichikawa 2005). The changes of sea level caused by the Kuroshio can reach up to around 10 cm along the south coast of Japan (Usui et al., 2011). For variations along the south coast of Japan, one interesting phenomenon is that during LM periods, the temperature along the south coast of Japan is relatively warmer than the NLM periods.

In recent years, coastal warming off the Tokai-Kanto district inside LM is frequently found, and local atmospheric responses to it have been studied. (Sugimoto et al., 2019, 2021). In Figure.1.5, the weekly SST field shows the marked coastal warming phenomenon off Tokai.

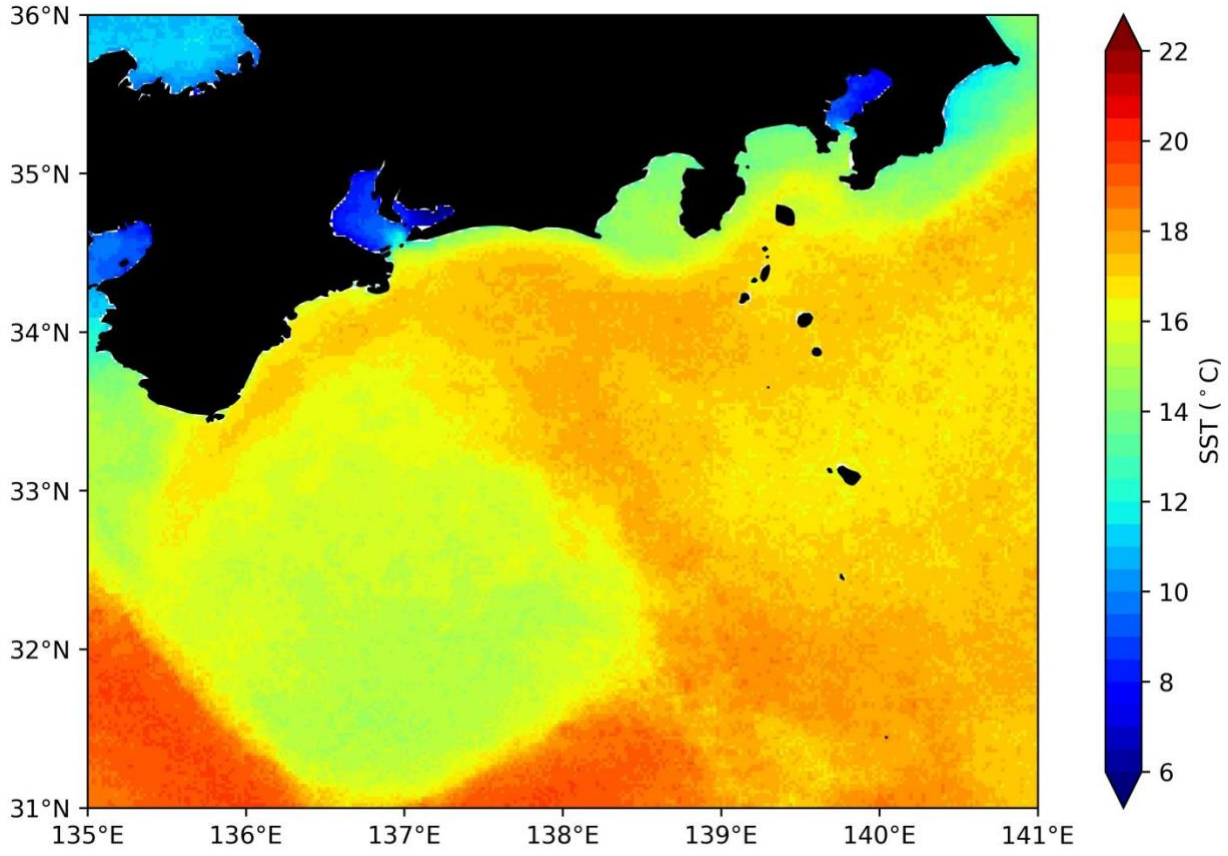

Figure.1.5 Weekly SST(°C) from 2019.01.31 to 2019.02.06

Although coastal warming events are widely considered to be generated by the Kuroshio, their mechanisms remain unclear. One important reason is that the ocean signal which related to these events have been smoothed out in gridded SSH data.

The reason is associated with the production of gridded SSH data. Different satellite altimeters can observe the area of the earth by footprint. The size of the footprint is determined by the location of the satellite in its orbit, the shape and size of beam produced by its transponder ,and also has something to do with the distance from the earth.

Since the spatial coverage of the footprint of one satellite altimeter is sometimes limited, researchers tend to process satellite data into gridded dataset. Gridded SSH data is produced from multi-mission satellite dataset with different temporal and spatial resolution. The interpolation is applied to produce gridded SSH data, so that much individual information is removed in gridded SSH data and it could not be very suitable to describe some fast-moving or small-scale ocean phenomenon.

Thus, in this study, We make full use of the advantages of along-track SSH data. we investigate coastal warming events inside the Kuroshio LM. Besides, we also consider the LM reference when calculate the anomaly of SST and SSH.

2. Data and Methodology

2.1 Gridded SST and data processing

2.1.1 Gridded SST data

Himawari-8 L3 gridded SST product is used. Himawari-8 satellite entered operational service on 7 July 2015 and carries an Advanced Himawari Imager (AHI) (Figure.2.1) scanning five areas: Full Disk (images of the whole Earth as seen from the satellite), the Japan Area (Regions 1 and 2), the Target Area (Region 3) and two Landmark Areas (Regions 4 and 5). The Target Area and Landmark Areas are not fixed and can change according to meteorological conditions.

Figure.2.2 shows the first true-color composite image from Himawari-8 at 02:40 UTC on 18 December 2014. In each 10-minute period, the Full Disk is scanned once, the Japan Area and Target Area are scanned for four times and the Landmark Areas are scanned for twenty times. The division of 10 minutes is the basic unit of an observation schedule, which is called a timeline. Figure.2.3 shows scan images on a timeline. Table.2.1 shows the observation frequencies of five areas.

Figure.2.1 Himawari-8 units, from Bessho et al. (2016)

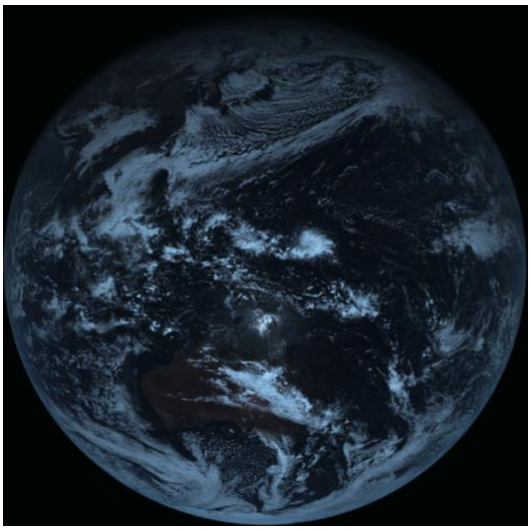

Figure.2.2 First true-color composite image from Himawari-8 at 02:40 UTC on 18 December 2014, from Bessho et al. (2016)

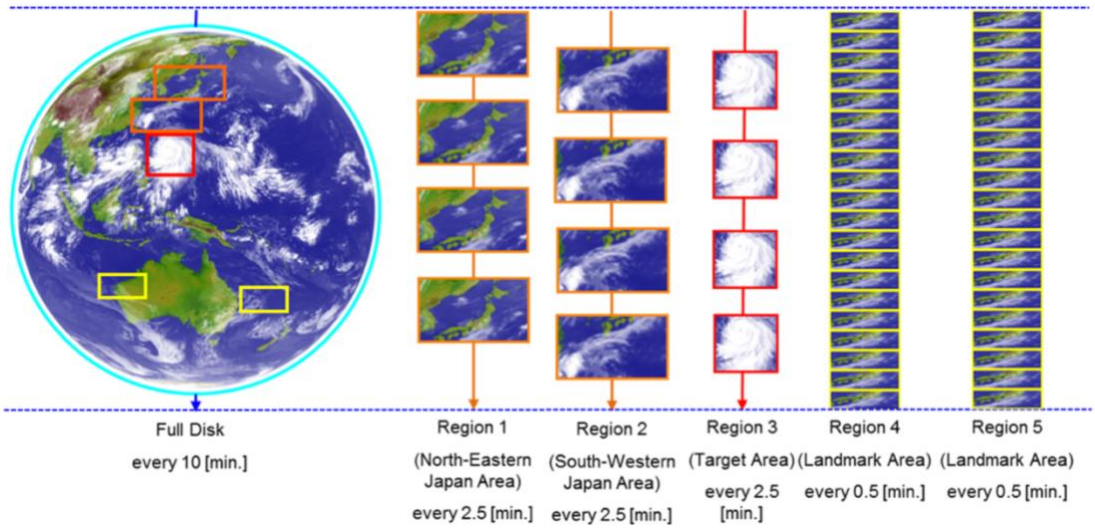

Figure.2.3 Himawari-8 scan images on a timeline, from Himawari Standard Data User's Guide V1.3

Observation area	Observations per timeline	Time cycle (min)	Observations per day
Full Disk	1	10	144
Japan Area	4	2.5	576
Target Area	4	2.5	576
Landmark Area	20	0.5	2880

Table.2.1 Himawari-8 observation frequencies of five areas, from Himawari Standard Data User's Guide V1.3

Research product of Himawari-8 L3 SST gridded (produced from Himawari-8) that used in this paper was supplied by the P-Tree System, Japan Aerospace Exploration Agency (JAXA). JAXA's P-Tree system, that provides multi-satellite products, releases the geostationary satellite Himawari-8 Standard Data provided by the Japan Meteorological Agency (JMA) as well as the geophysical parameter data produced by JAXA using the Himawari-8 Standard Data.

For SST data, the Himawari-8 gridded product basically has several levels of data with different temporal resolution:10-minutes (Level 2), 1-hour (Level 3),1-day (Level 3), 1-month (Level 3). In our study, we use the daily gridded data. It is the "daily minimum SST" calculated from hourly data, which is generated from 10-minute data (Level 2) with quality level.

In previous studies, SST data from satellite remote sensing observation and in situ observation (ships, drifting buoys, Argo floats, etc.) are widely used. Compared with the in-situ method, the Himawari-8 satellite observation method can cover large areas of sea surface and has a high spatial resolution with 2 km. The high spatial resolution is suitable for researchers to better describe some ocean phenomenon, such as our study of coastal warming events.

The Himawari-8 SST gridded data we use is only available from June 2015. To calculate long-term mean of SST, which is another reference in the present study to obtain SST Anomaly (SSTA), we additionally use the Optimum Interpolation Sea

Surface Temperature (OISST) data from January1993 to September 2012. OISST incorporates observations from various platforms (satellites, ships, buoys, and Argo floats) and has a temporal resolution of one day and a spatial grid resolution of 0.25° (Banzon et al., 2020; Huang et al., 2021).

2.1.2 Gridded SST data processing

The gridded daily Himawari-8 SST data is averaged over 7 days to get the weekly SST data for the following two reasons. First, due to great variations in cloud coverage and heat flux, missing SST data in each grid can be frequently found and the daily SST value fluctuates greatly within a few days. Figure.2.4 shows weekly mean SST from 2018.05.13 to 2018.05.19, in which few missing data can be found. Second, coastal warming event has a temporal scale of a few to several weeks, making weekly data suitable for coastal warming event studies.

The start day of weekly SST field depends on the period of coastal warming events we study. The details are listed in the next chapter. Besides, since we want to study the coastal warming events during LM period, here we dare to use LM period (2017.09.01-2019.04.13) mean to calculate the SST Anomaly (SSTA).

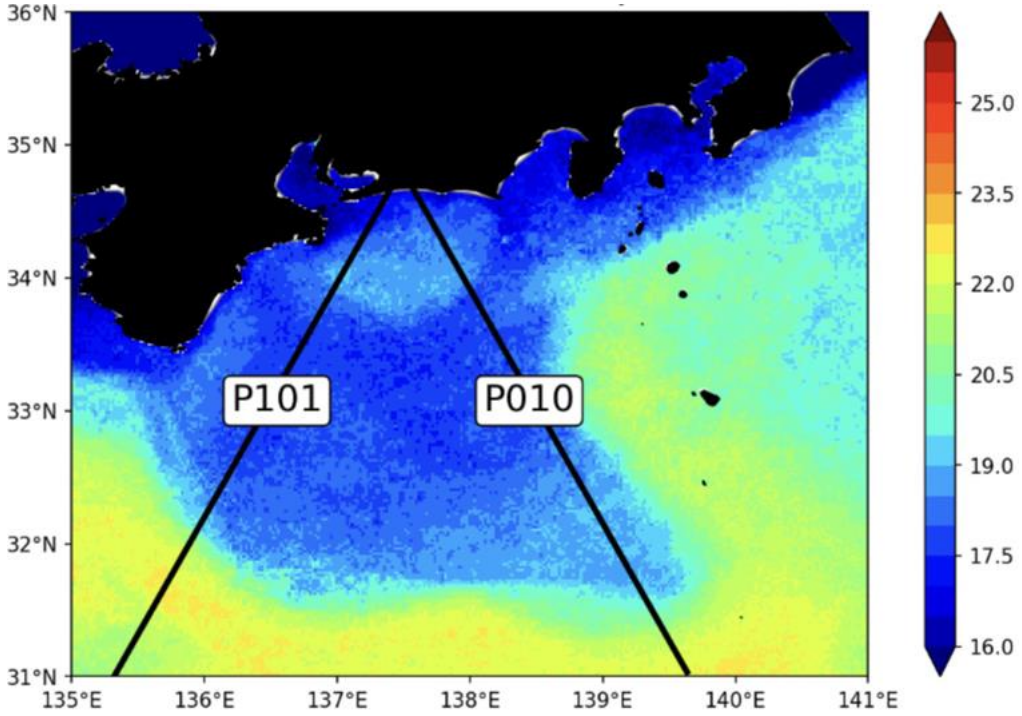

Figure.2.4 Weekly mean SST (°C) from 2018.05.13 to 2018.05.19

Because the observation of coastal warming events phenomenon can be affected by seasonal variation of temperature, SSTA is not the most suitable way to distinguish coastal warming events. Thus, we define the Sea Surface Temperature Anomaly Difference (SSTAD), which is the difference between SSTA in each grid and the area-mean SSTA (30.5°N -31.5°N, 133.5°E -135.5°E) within the same period.

The purpose of taking area difference is to better find coastal warming events, through seperating the seasonal variation related factors.The area we select (30.5°N -31.5°N, 133.5°E -135.5°E) satisfies the following 4 standards:

1. Outside the Kuroshio LM, which means this area should not be affected by the Kuroshio or Kuroshio Extension.
2. No effect of passing eddies.
3. Time series of area-mean SST shows good seasonal variation.
4. Latitude between 30°N and 35°N.

Based on the above criteria, we select 2 reasonable areas and compare their SST variations. In 3.2.5, green curve represents Wakasa Bay (regard as seasonal variation of SST),which is the area-mean used as a validation tool. Orange curve represents the selected region (30.5°N -31.5°N, 133.5°E -135.5°E) in our study, and blue color represents the compared region.

Compared with blue curve, the temporal variation of orange curve is more close to the green curve (the variation trend of phase), which indicates that the area of orange curve has a more clear characteristic of seasonal SST variation. As a result, we decide to use the region (30.5°N -31.5°N, 133.5°E -135.5°E), as a suitable reference in our study. In Figure.2.6, the above region is marked as a red box.

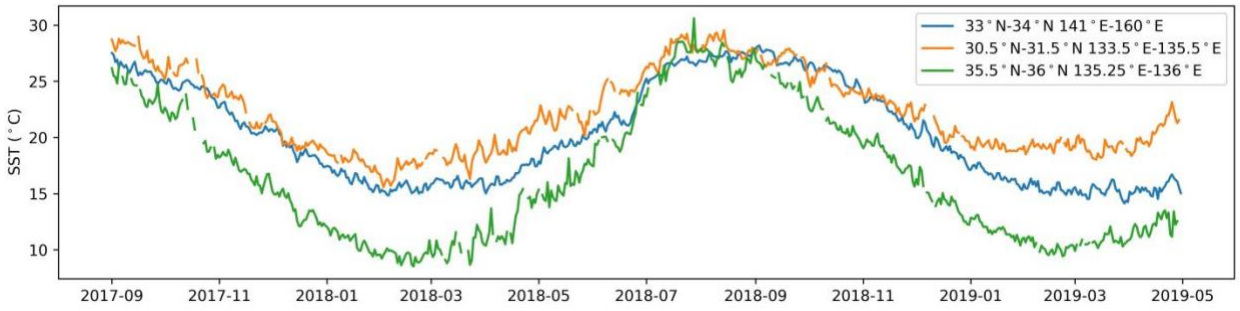

Figure.2.5 Time series of area-mean SST (°C) in Wakasa Bay and 2 regions

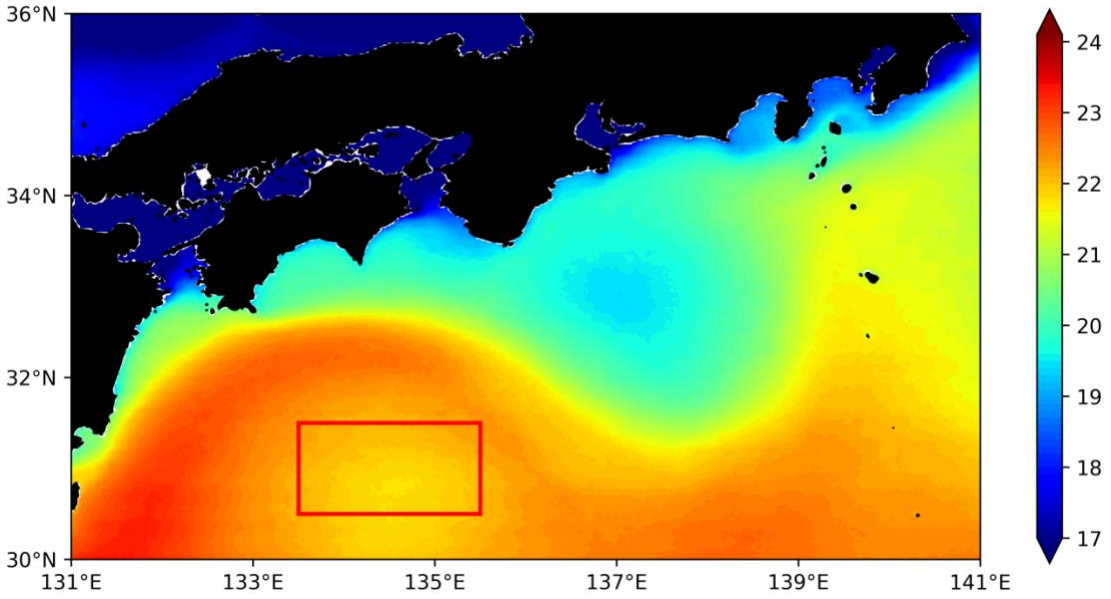

Figure.2.6 Sea Surface Temperature (°C) during LM period. Red box represents the reference area we selected and then used to calculate the area mean

After taking the area difference, we first define SSTAD as the following one:

$$SSTAD = SSTA - SSTA_{area-mean} + c$$

Here, c is the constant used to adjust the value of SSTAD, to make the SSTAD field much easier to describle coastal warming events.

In Figure.2.7, we find that the value of "$SSTA - SSTA_{area-mean}$ "around 0 °C is easy and suitable to distinguish coastal warming events.Thus, the c is determined as 0 in the above formula. Next, we apply the linear interpolation to gridded SSTAD data along Pass 010 and Pass 101, to get the along-track SSTAD Hovmöller diagrams.

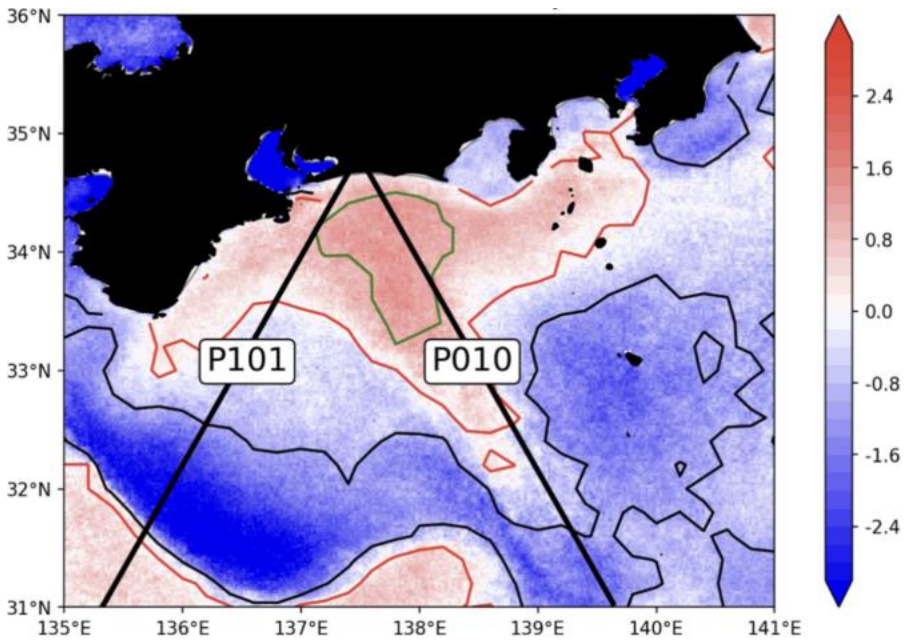

Figure.2.7 The value of SSTA $-$ $\mathrm{SSTA}_{\mathrm{area-mean}}$ when coastal warming event happened. Black, red, green contour line refer to -1°C, 0°C,1°C

2.2 Along-track SSH and data processing

2.2.1 Along-track SSH data

Jason-3 along-track SSH data is used to analyze the coastal warming event. The Jason-3 data we use has the temporal resolution of 10 days. We use both Pass 010 and 101, which pass over the area south coast of Japan.

Figure.2.8 shows the locations of 2 along-track pass of Jason-3. When it comes to the different cycle of same pass, the observation point is not the same, but its difference is relatively small (less than 1 km) and can be neglected compared with the spatial size of phenomenon we want to study.

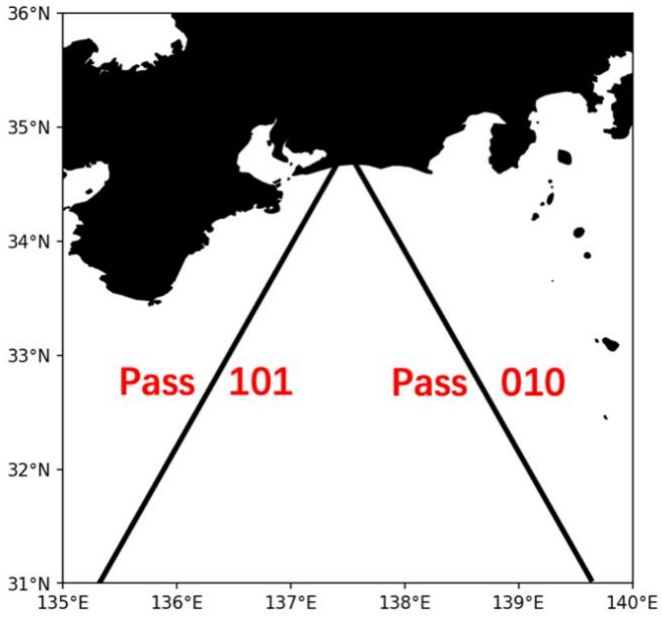

Figure.2.8 Locations of along-track Pass 101 and Pass 010

The along-track SSH data in our study were produced by the Deutsches Geodätisches Forschungsinstitut (DGFI-TUM). Data are provided at high-frequency (hf) and low frequency (lf). lf is the post-processed measurements derived from the hf and provides one sea level measurement roughly every 7 km. lf data are generally used in research about sea level variations and are also used in our study. The data of all missions have been cross-calibrated in advance (following the approach of Bosch et al., 2014; referenced to Jason-1) and are corrected for radial errors.

Besides, Adaptive Leading Edge Subwaveform (ALES) algorithm is applied to the satellite SSH data. Data in the coastal ocean are much improved, and the SSH data are also reliable in the open ocean.

Thus, coastal accuracy has been improved and guaranteed when we use ALES-reprocessed along-track SSH data, which can help us better describe coastal warming events and make the result more persuasive. Figure.2.9 is the flow diagram of ALES retracking procedure for each waveform.

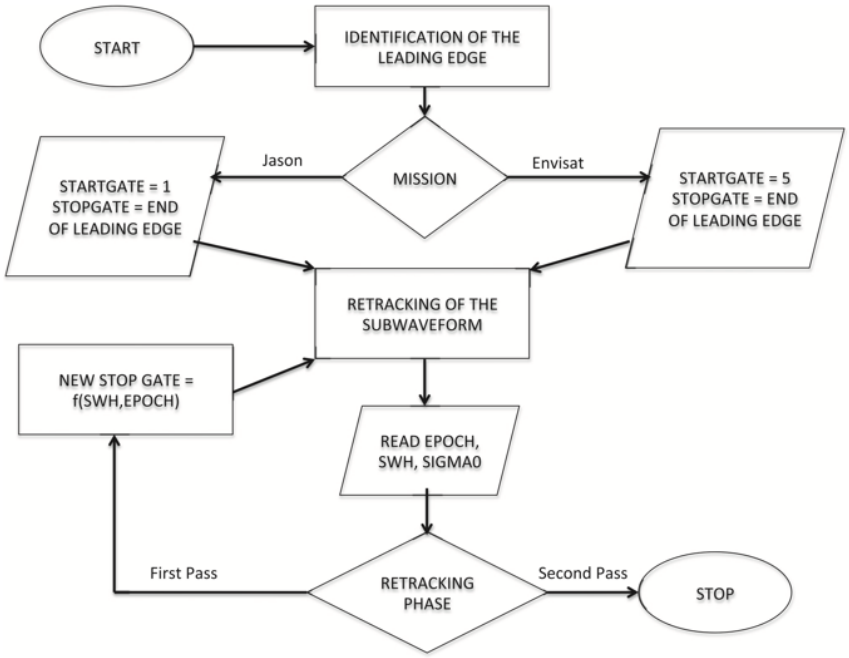

Figure.2.9 Flow diagram of ALES retracking procedure for each waveform. Startgate and stopgate refer to the starting gate number and end gate number of the subwaveform window, from Passaro et al. (2014)

2.2.2 Along-track SSH data processing

The SSH anomaly (SSHA) was calculated using the following formula based on the LM period reference (2017.09.01-2019.04.13) to highlight coast warming events inside the LM.

We use the following formula to calculate SSHA:

$$SSHA = SSH - MSS - Load\ Tide - Ocean\ Tide,$$

where MSS refers to mean sea surface height during the LM period (2017.09.01-2019.04.13).Then, we performed data quality control (QC) according to the ALES web's suggestion:

- |SSH-MSS| > 2.5 m
- SWH > 11 m
- stdalt > 0.20 m

To control the quality of data ,we removed some abnormal data ,which is out of normal range. we define the value's normal range of SSHA [-1.8m, 1.5m] and value's normal range of Dssha [0, 0.2m]. (Dssha: SSHA Difference of two spatial adjacent points, could be regarded as the same function of geostrophic velocity's QC standard). After QC, we interpolated it. During the process of interpolation, we also considered the effect of islands and lands and removed them.

2.3 Gridded SSH and data processing

2.3.1 Gridded SSH data

To calculate SSHA Difference (SSHAD) later in the same way as SSTAD, the area-mean SSHA is needed. Since along-track SSH data can not be used to calculate the area-mean SSHA,here, AVISO gridded Sea Level Anomalies (SLA) product is used.

Along-track (L3) products are calculated from the difference between the instantaneous SSH and a temporal reference. This temporal reference can be a Mean Profile (MP) in the case of repeat track or a gridded Mean Sea Surface (MSS) when the repeat track cannot be used. The computation of the SLAs and their associated errors are detailed in Dibarboure et al. (2011) and Pujol et al. (2016).

2.3.2 Gridded SSH data processing

AVISO gridded data is used to calculate the SSHA mean (30.5-31.5°N, 133.5-135.5°E) during LM period. Note that we choose the LM period reference when calculating the anomaly of temperature and height, but the original SSHA data from AVISO is based on the long-term reference (1993-2012).

So, we process the SSHA data: SSHA (LM reference) =SSHA (from AVISO,1993-2012 reference) – LM period average of SSHA (from AVISO,1993-2012 reference). By doing this job, the SSHA based on LM reference is prepared to use.

We assume that the monthly SSHA refers to the SSHA on 15th of every month, then we apply the linear interpolation to get daily SSHA data, to match the date of along-track SSHA data.

Then, we calculate the Sea Surface Height Anomaly Difference (SSHAD) as SSTAD's methodology by using the along-track SSHA data and gridded SSHA data, we define the SSHAD as the following one:

$$SSHAD = SSHA_{ALES} - SSHA_{AVISO,\ area-mean}$$

3. Results

3.1 Two cases of coastal warming event

Here, we define the coastal area of Tokai district (CAT;33.5°–34.5° N, 136.5°–138.5° E), which is the same definition as (Sugimoto et al.2020).The along-track SSH data from Jason-3 is available from 2016.02 to 2019.04, and according to weakly SST figures(Figure.3.1 - Figure.3.5), there are many cases when the SST around CAT is warmer than the surrounding area.

We first consider the lasting duration of warm SST around CAT, as well as the continuity of temperature difference between CAT and the surrounding area.We find that the warm SST around CAT appeared frequently. But for many cases, they disappeared quickly and could not exist for more than one month.In general, the time scale of coastal warming events during our selected LM period is short, also accompanied with limited spatial size.

Since we want to study coastal warming events with long duration, during which more information and characteristics could be found, two cases of coastal warming event (2018.12-2019.03, Case I; 2018.05-2018.06, Case II) are selected and studied.

These 2 cases are chosen from many cases have, and they both have sufficient durations and the warm SST around CAT is easy to distinguish. Besides, they continued to exist for more than one month.

During Case I and Case II periods, the Kuroshio axis both varied greatly, but the movement areas for two cases are different. And the generation and propagation of coastal warming events are also different for two cases.

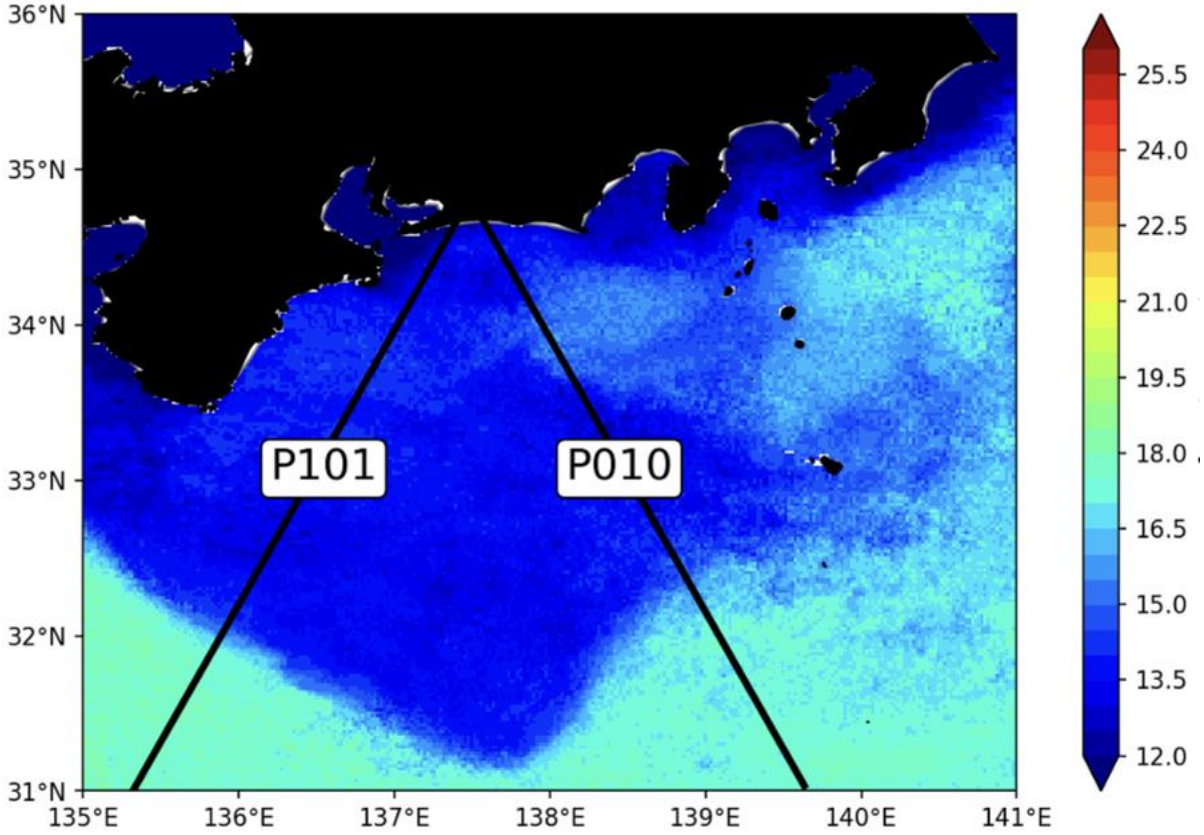

Figure.3.1 Weekly Sea surface temperature (°C) from 2018.02.17 to 2018.02.23

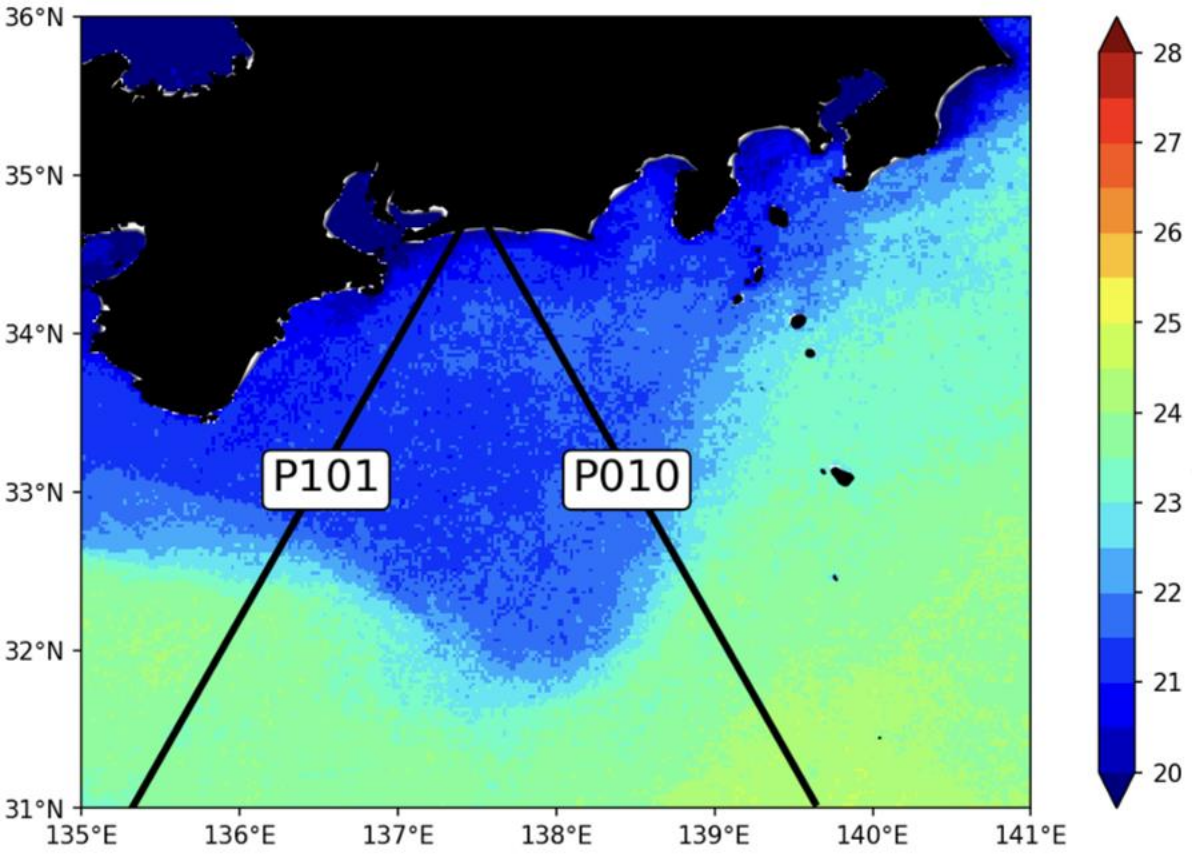

Figure.3.2 Weekly Sea surface temperature (°C) from 2018.11.07 to 2018.11.13

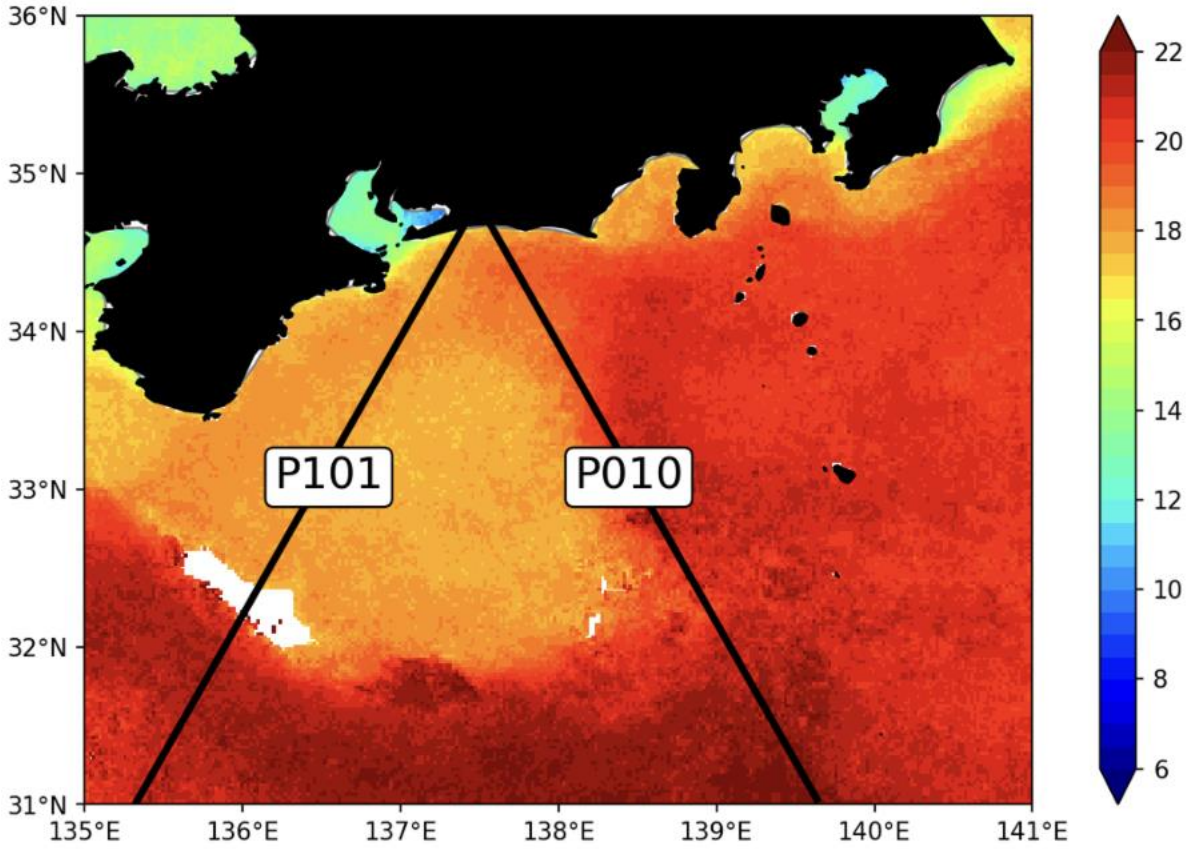

Figure.3.3 Weekly Sea surface temperature (°C) from 2018.12.13 to 2018.12.19

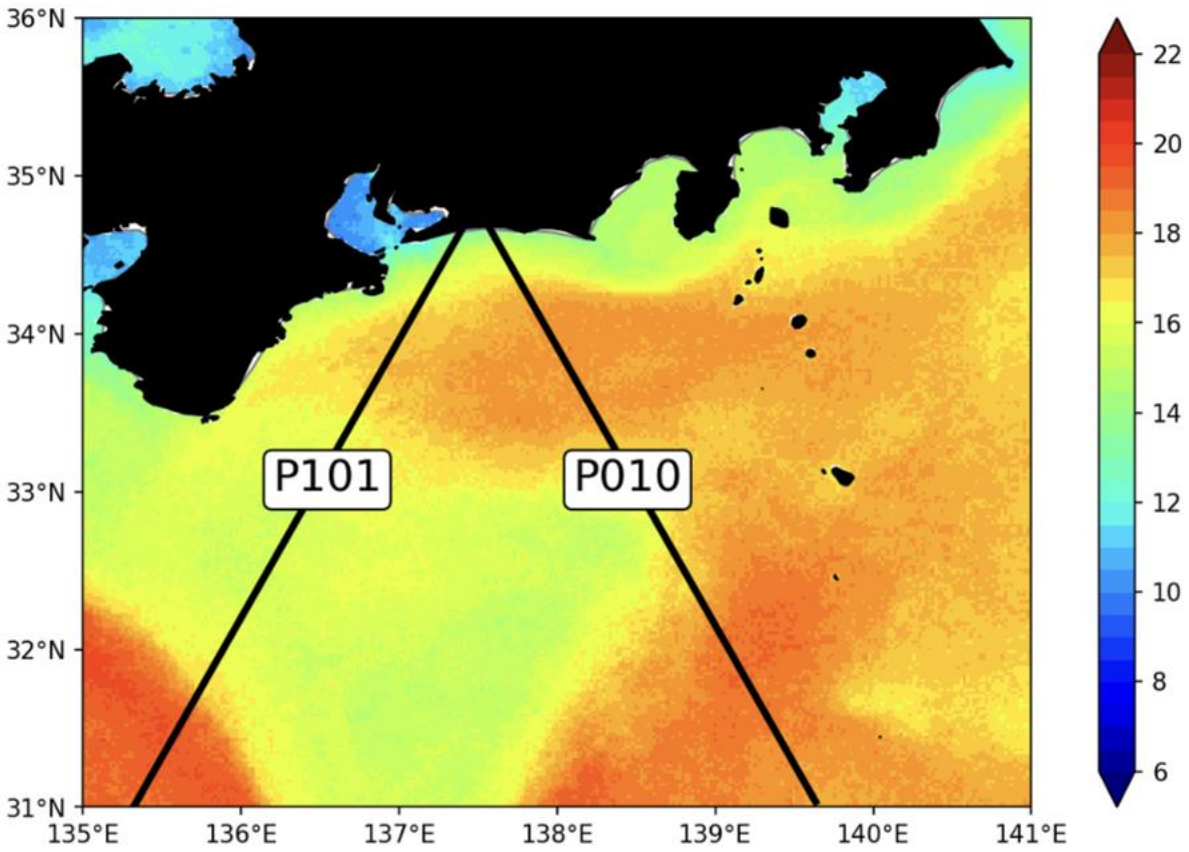

Figure.3.4 Weekly Sea surface temperature (°C) from 2019.04.04 to 2019.04.10

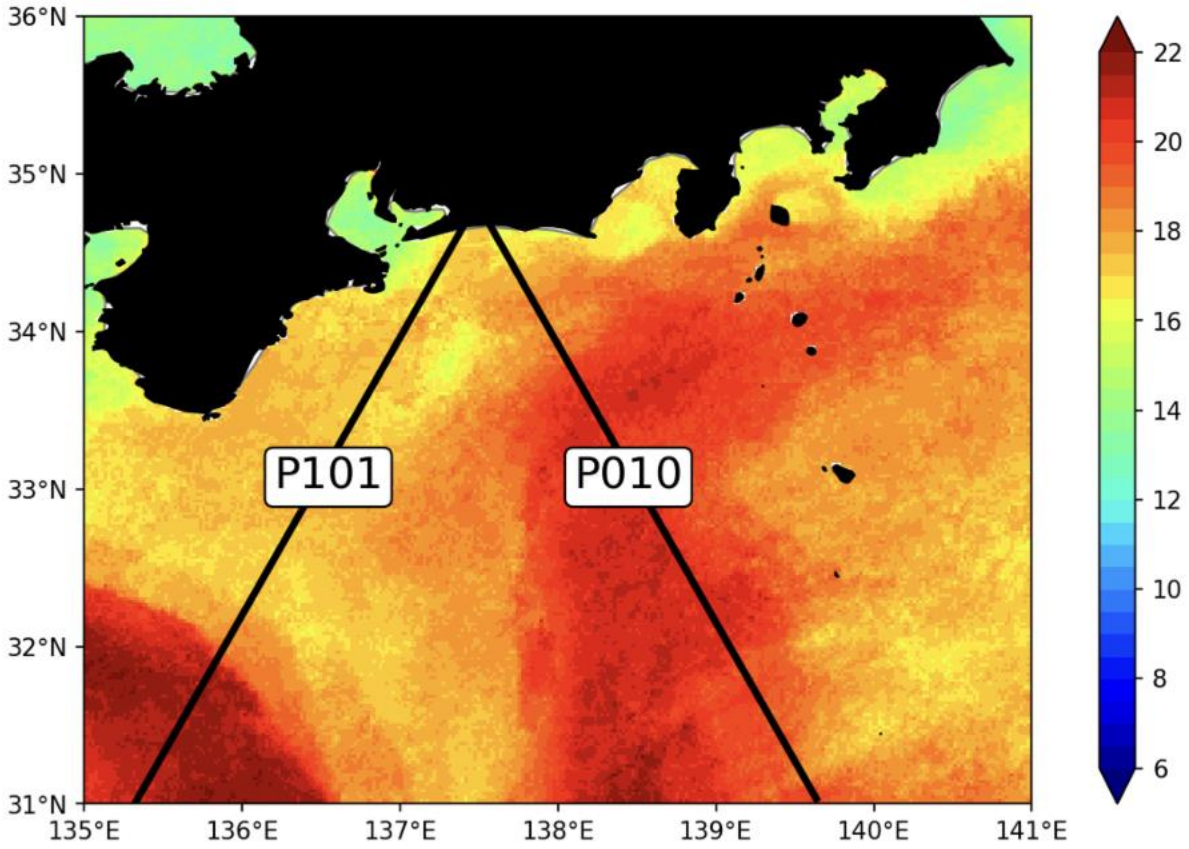

Figure.3.5 Weekly Sea surface temperature (°C) from 2019.04.25 to 2019.05.01

3.2 Case study I for coastal warming event

3.2.1 For SSTAD and SSHAD

For Case I of coastal warming event, we focus on the period from December 2018 to March 2019. The SST field (Figure.3.6-Figure.3.8) reveals Case I of coastal warming event off Tokai.

The Figure.3.7 shows marked coastal warming off the Tokai to Kanto districts, where the SST is warmer than the surrounding area, the difference could be around 1-2°C. Besides, the shape of the Kuroshio front largely changed along Pass 010. The northwest movement of the Kuroshio front is recognized along Pass 010.

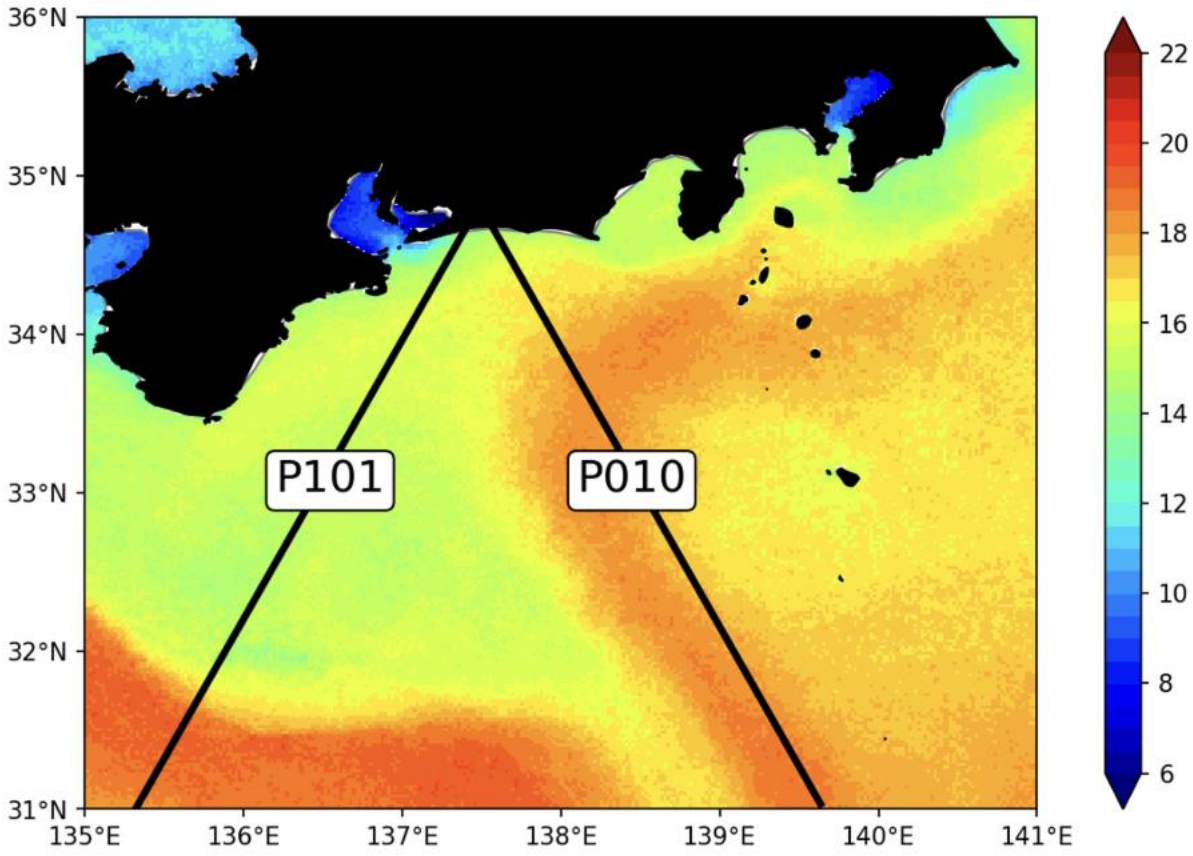

Figure.3.6 Weekly Sea surface temperature (°C) from 2019.01.24 to 2019.01.30

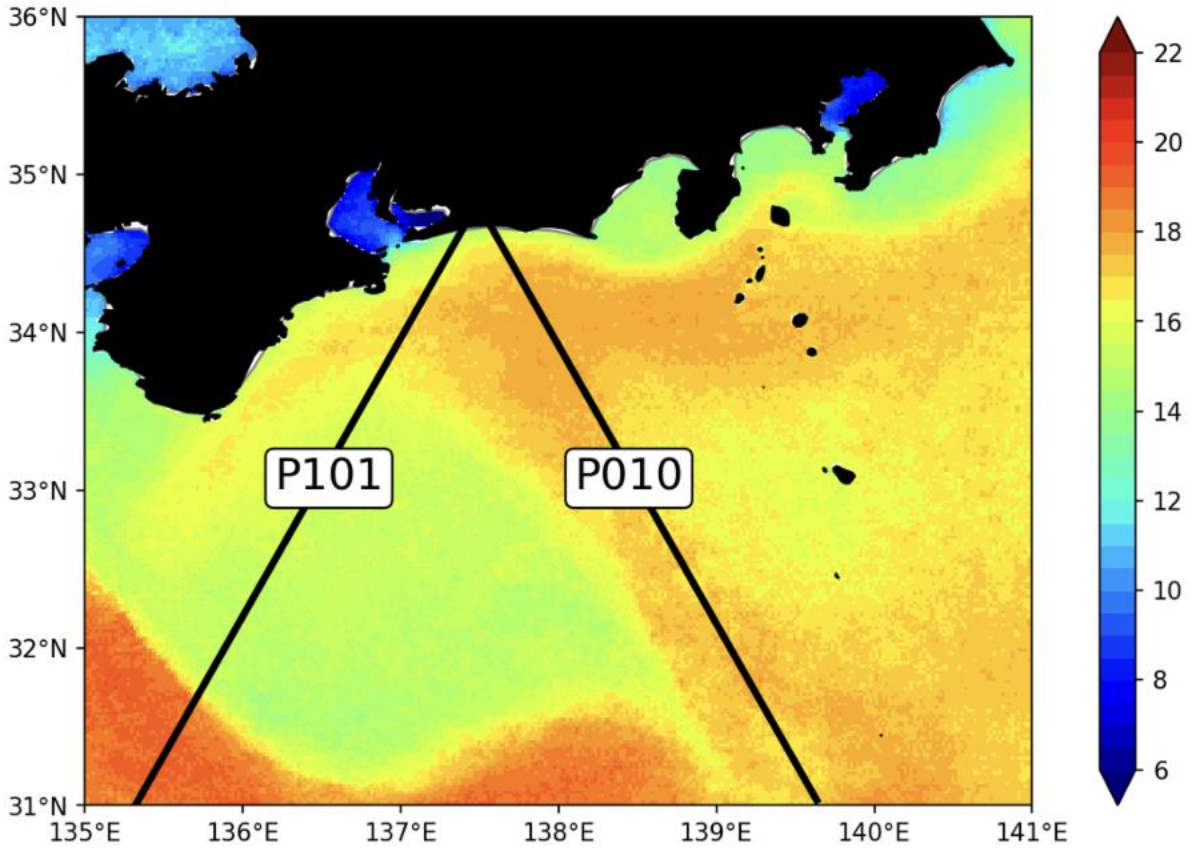

Figure.3.7 Weekly Sea surface temperature (°C) from 2019.01.31 to 2019.02.06

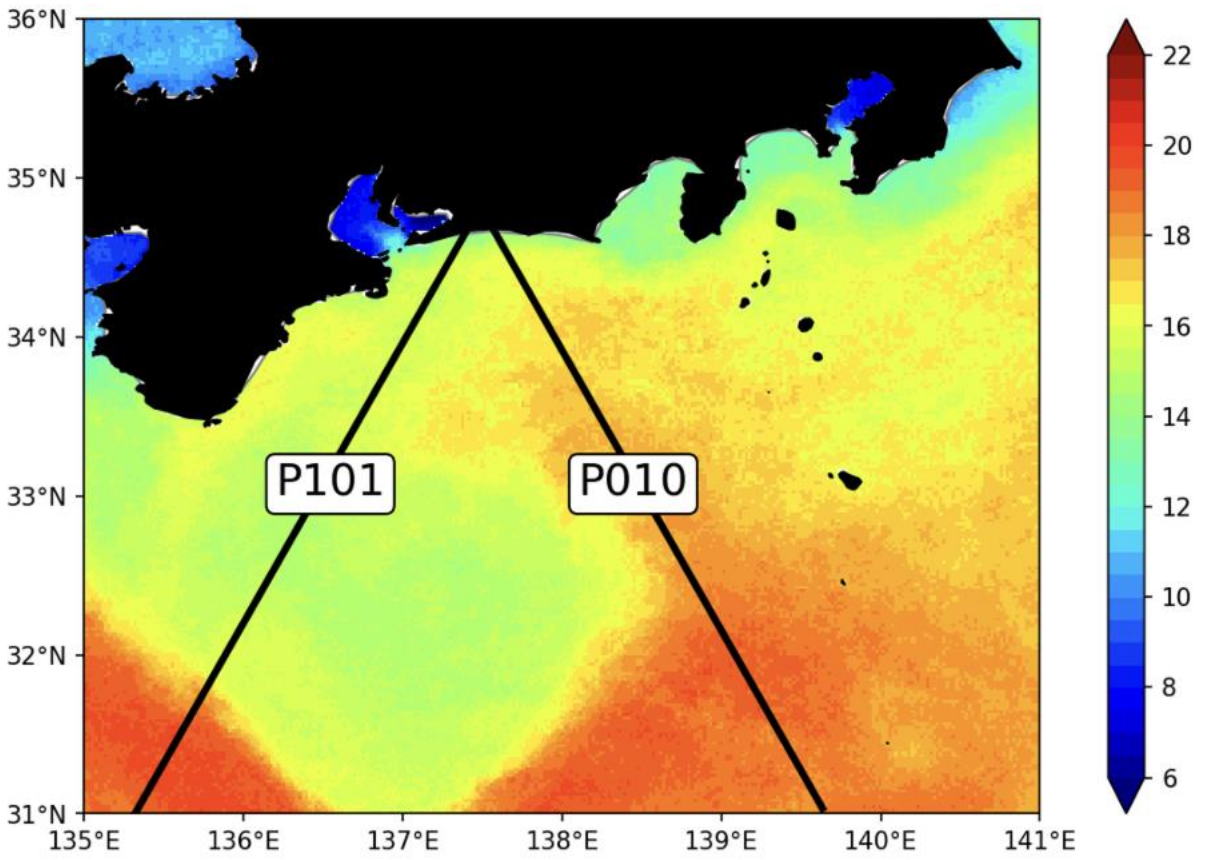

Figure.3.8 Weekly Sea surface temperature (°C) from 2019.02.07 to 2019.02.13

Hovmöller diagram of SSTAD along Pass 010 also shows the northward movement of Kuroshio front (Figure.3.9). During the period from 2019.01.10 to 2019.02.11, pay attention to the latitude from 32.5°N to 34.5°N in the following SSTAD field. We can find a northward signal. This positive signal is around 2°C, which is consistent with the result in SST field (Figure.3.6-Figure.3.8).

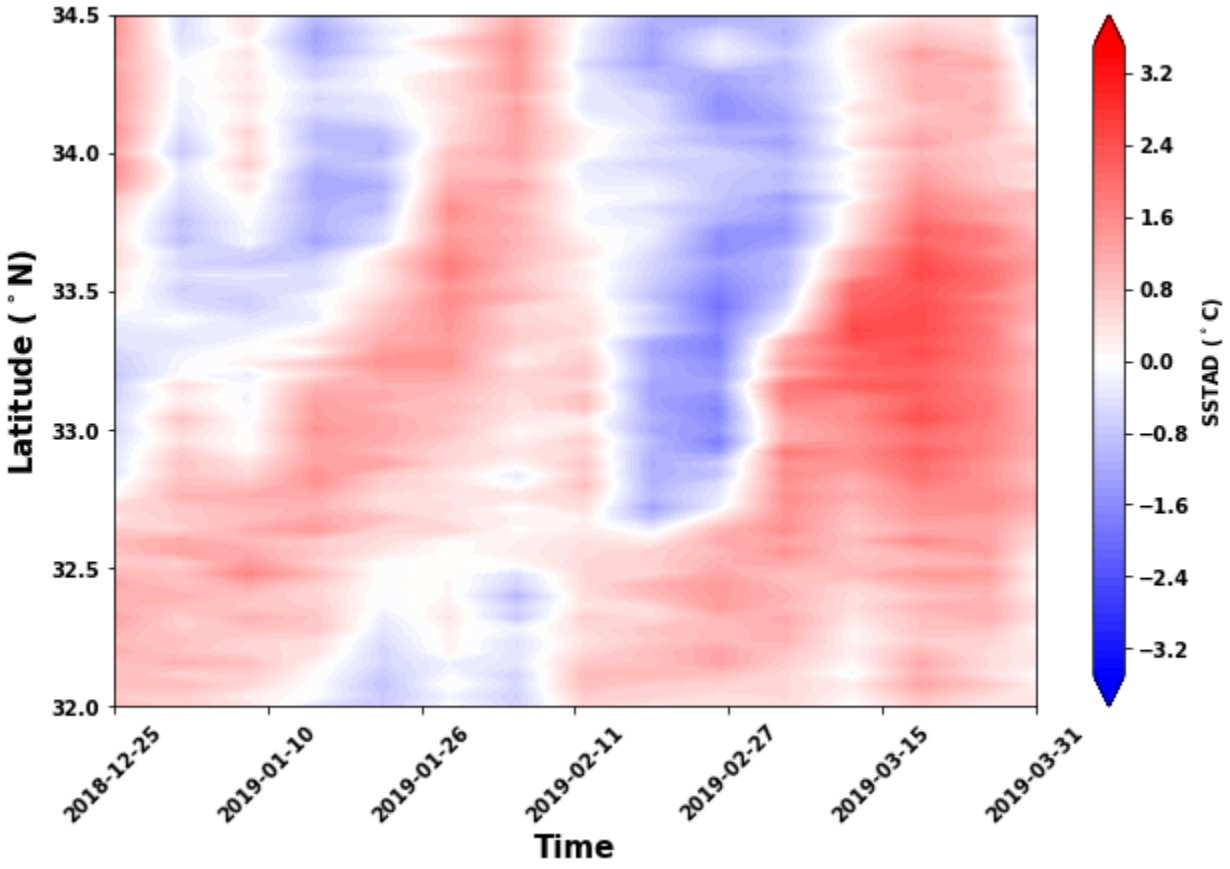

Figure.3.9 Hovmöller diagram of SSTAD along Pass 010 for Case I

Figure.3.10 is the Hovmöller diagram of SSHAD along Pass 010. The contour interval is 0.1 m. During the period from 2019.01.10 to 2019.02.11, we also focus on the latitude from 32°N to 34.5°N in the following SSHAD field. The similar northward signal could also be found. This signal is significant.

Combining the signal of in SST, SSTAD and SSHAD diagram, the great variation of Kuroshio axis in the area between 32°N and 33.5°N can be clearly found.

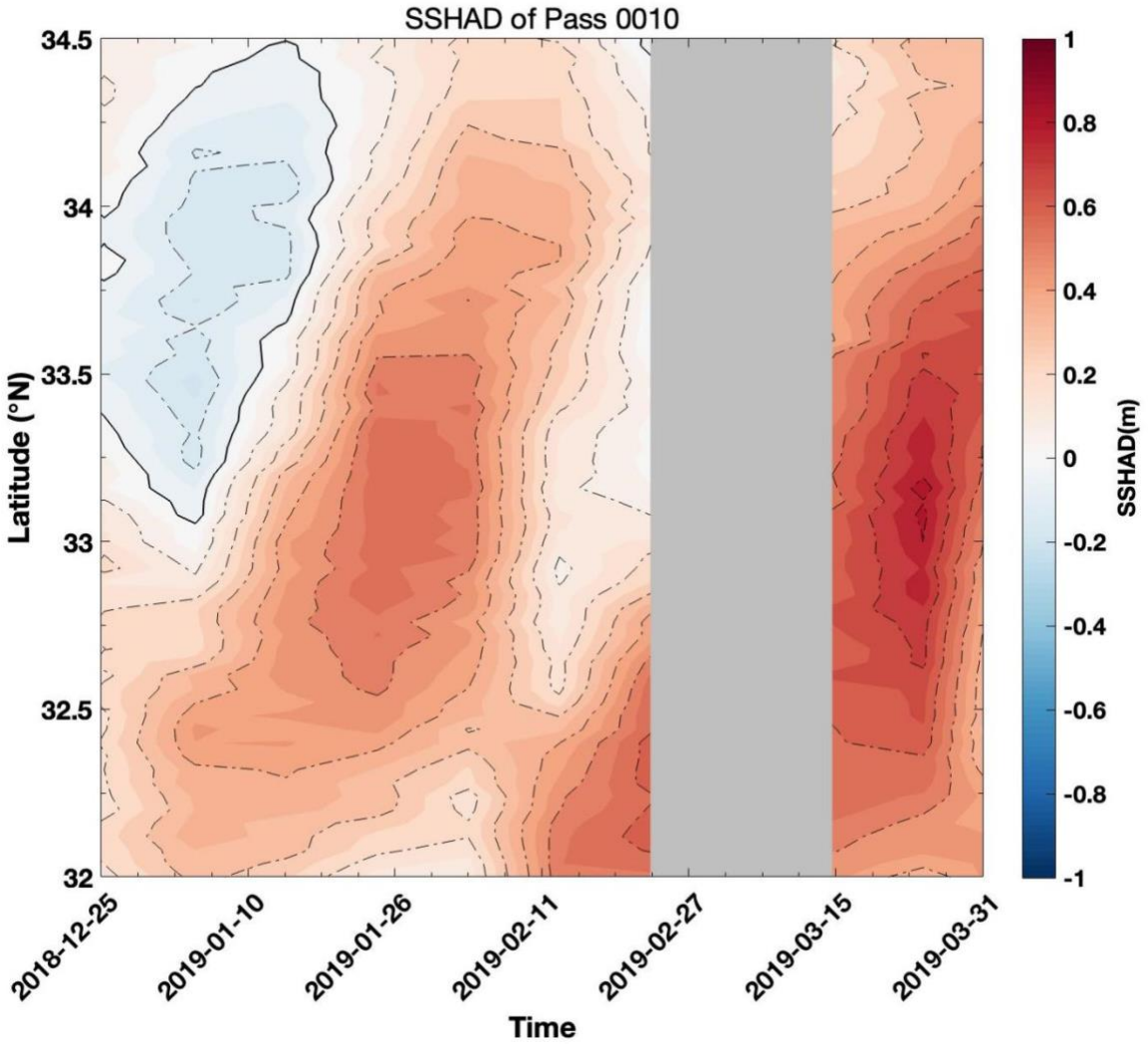

Figure.3.10 Hovmöller diagram of SSHAD along Pass 010 for Case I

Since the coastal warming event in Case I is indicated as the westward movement of warm water around 33°N -34°N, we also examine SSTAD and SSHAD along Pass 101. Figure.3.11 is the Hovmöller diagram of SSTAD along Pass 101. The SSTAD shows the similar tendency with the SST figures.

We focus on the same period and the same range of latitude as above, finding that the positive SSTAD value only existed in the area which is north than 33.5N. Compared with the positive value for Pass 010, the signal is weaker (The max value is around 0.8°C).

One possible reason could be coastal warm water gets weaker during the process of propagation. It is possible that the distance between Pass 010 and Pass 101 in our study area (up to around 100 km) may cause it.

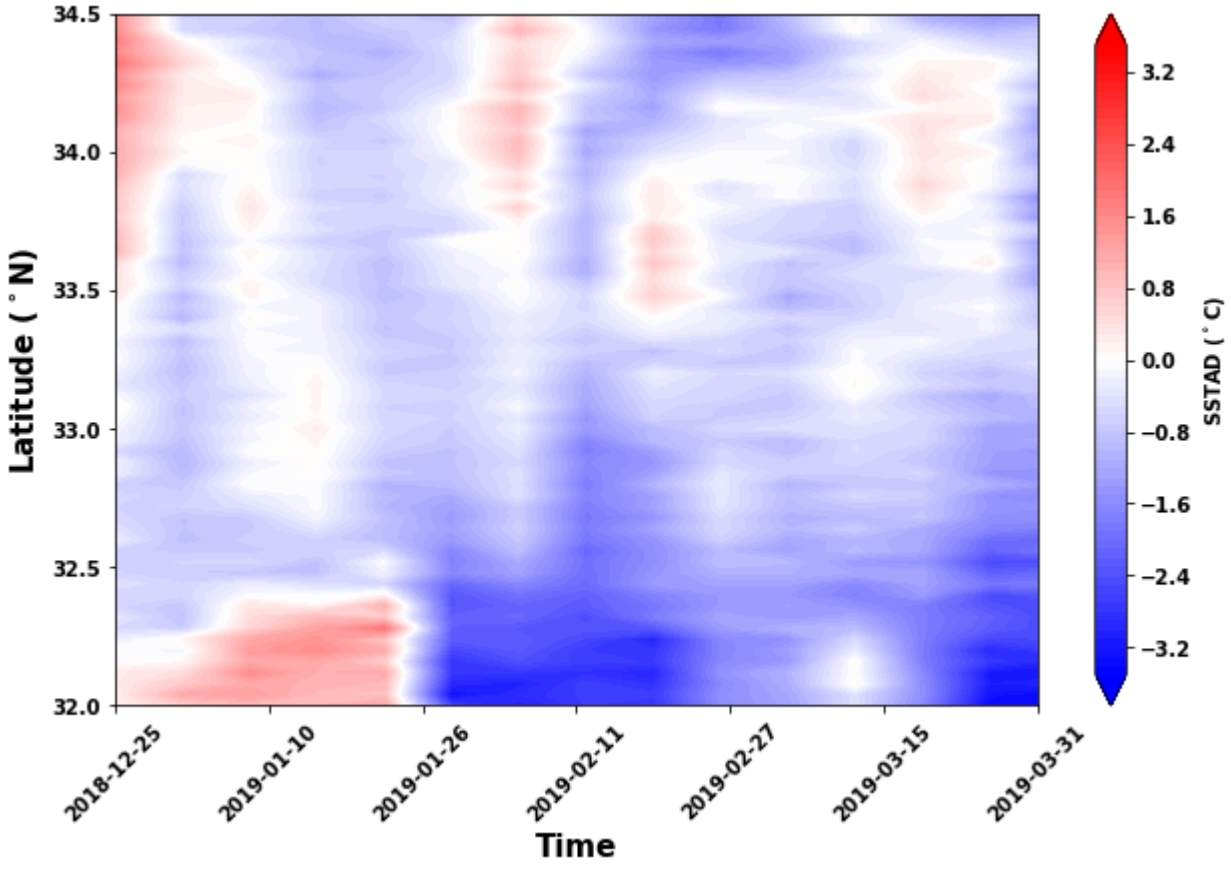

Figure.3.11 Hovmöller diagram of SSTAD along Pass 101 for Case I

Figure.3.12 is the Hovmöller diagram of SSHAD along Pass 101.We choose the area from 33.5N to 34.5N in SSHAD field, and the positive signal appeared from the day of 2019.01.26, also find that the signal between the SSHAD and SSTAD also has a similar tendency.

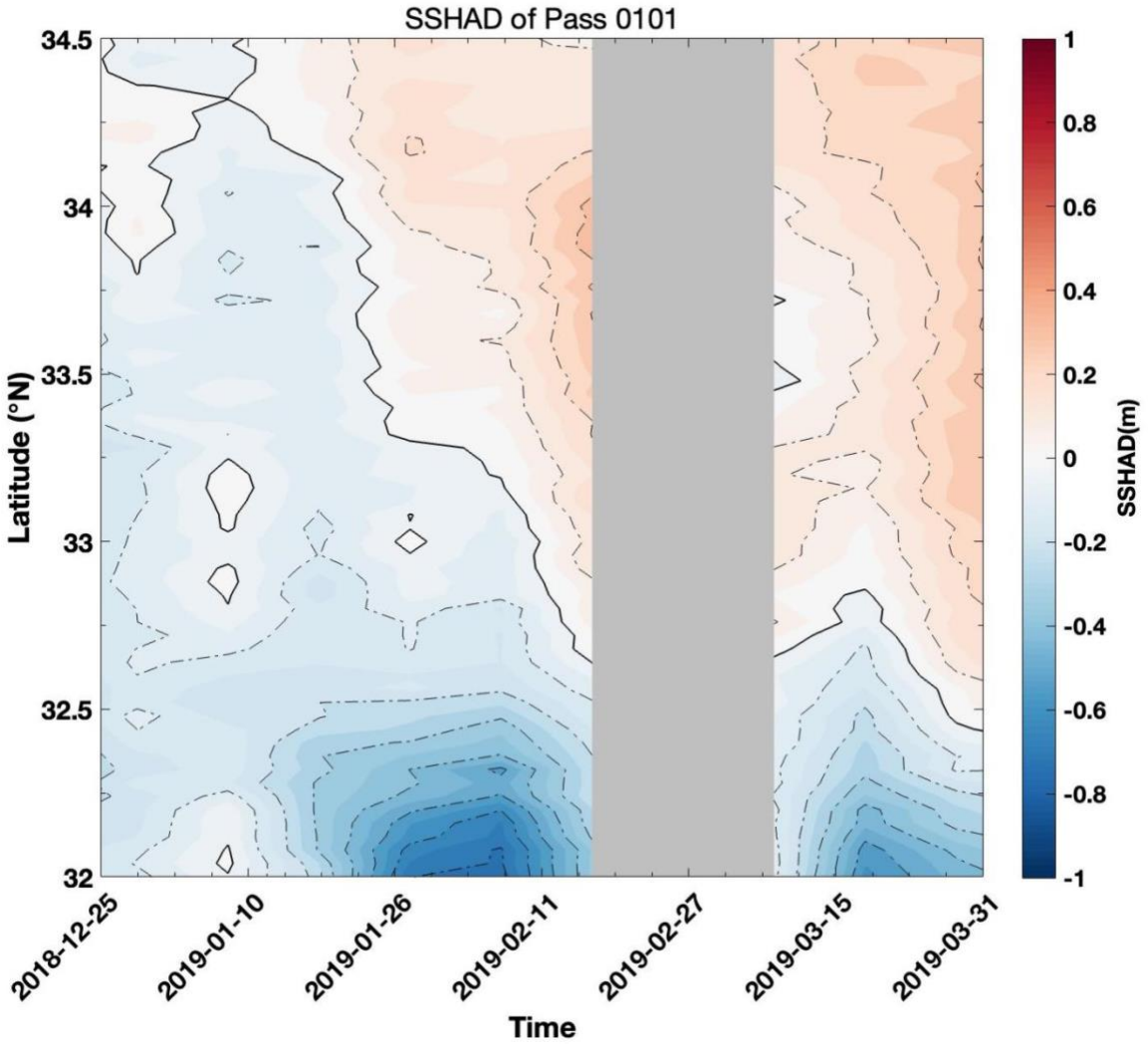

Figure.3.12 Hovmöller diagram of SSHAD along Pass 101 for Case I

3.2.2 Scatter Plot

To study the statistical relationship between SSTAD and SSHAD, the scatter diagrams are plotted along Pass 010 and 101. For Pass 010 and Pass101, we choose the latitude from 32 to 34.5N.

Here, k refers to regression coefficient and r refers to correlation coefficient. In the figures, statistically insignificant values at 95% confidence level are not shown.

Note that the SSTAD changes with the choice of the area, which is used to calculate area-mean SST reference.

Here, our definition: Case I of coastal warming event:

1. SSTAD > 0 °C
2. North than 34 °N

Figure.3.13 is the scatter diagram of SSHAD (m) and SSTAD (°C) along Pass 010.

In general, variation of SSHAD is positively correlated with the variation of SSTAD, consistent with the signals in Hovmöller diagrams of SSHAD and SSTAD.

And SSTAD varies from -2 °C to 3 °C, while SSHAD varies from -0.4m to 0.8m.

The scatter plot is divided into three slopes:

1) the slope between 32°N and 33°N, with the large k value of 0.108.
2) the slope between 33°N and 34°N, with the largest k value of 0.154.
3) the slope between 34°N and 34.5°N, with the small k value of 0.034.

In our opinion, the above characteristic and slope of scatter points between 33°N and 34°N are mainly caused by the northwest movement of Kuroshio axis, which had a great impact along Pass 010 during Case I period.

And for the area between 34°N and 34.5°N, the small k indicates that the SSHAD varies weakly with the change of SSTAD.

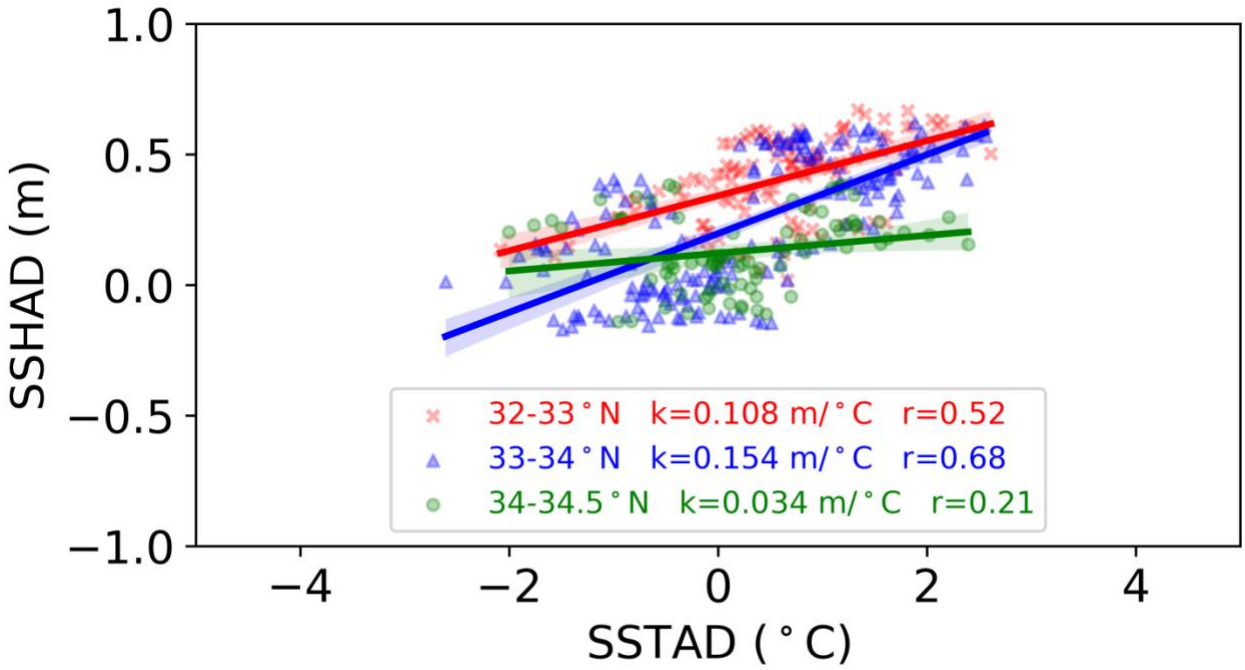

Figure.3.13 Scatter diagram of SSHAD (m) and SSTAD (°C) along Pass 010. Color represents the latitude

Figure.3.14 is the scatter diagram of SSHAD (m) and SSTAD (°C) along Pass 101.

Overall, the SSHAD along Pass 101 varies from -0.8m to 0.4m, while SSTAD along Pass 101 varies from -4°C to 2°C.

Then, two slopes of scatter points is divided:

1) the slope between 32°N and 34°N, with the large k value of 0.126.
2) the slope between 34°N and 34.5°N, with the modest k value of 0.056.

Here, the scatter points with different spatial patterns are also observed. The modest k indicates that SSHAD varies with SSTAD, but the amplitude is not as large as that of large k.

For scatter points between 34°N and 34.5N, the SSTAD and SSHAD are related to the coastal warming event. According to our definition, there are some scatter points with SSTAD>0 and positive SSHAD.

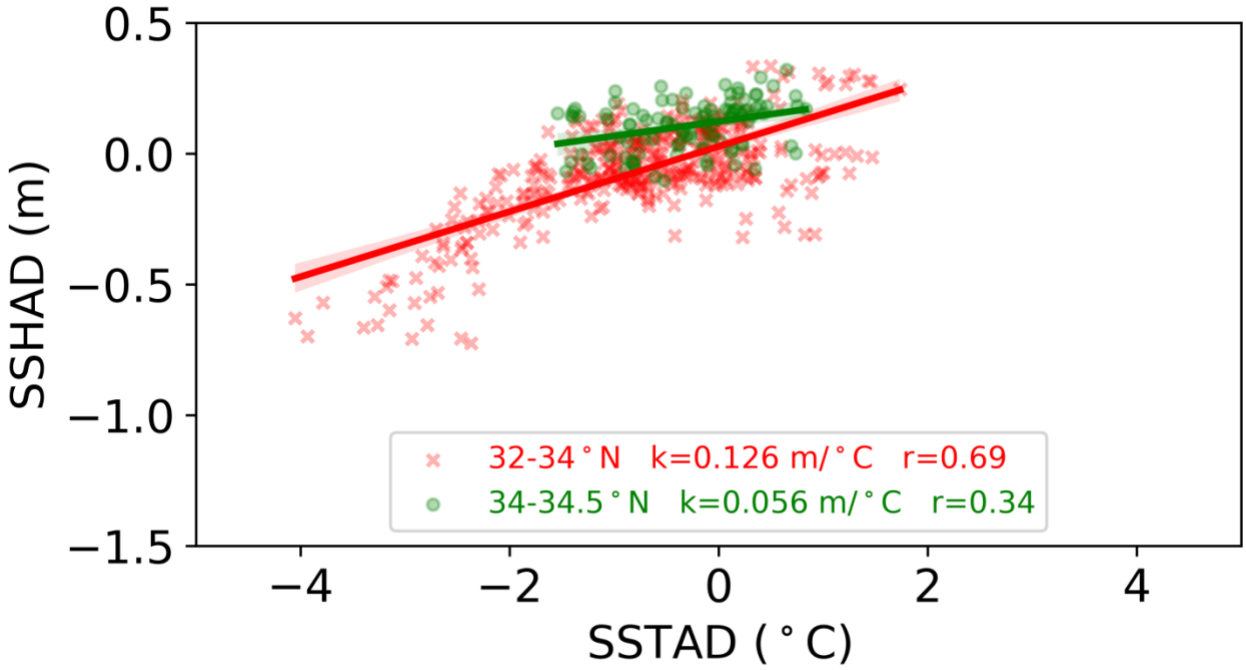

Figure.3.14 Scatter diagram of SSHAD (m) and SSTAD (°C) along Pass 101. Color represents the latitude

To conclude, for Case I of coastal warming event, the northwest movement of Kuroshio axis could be observed on Pass 010. And the scatter points in scatter plot also show the good correlation relationship. Then, the westward movement of warm water is observed on Pass 101.

3.3 Case study II for coastal warming event

3.3.1 For SSTAD and SSHAD

For Case II of coastal warming event, we focus on the research period from the May 2018 to June 2018. The SST field (Figure.3.15-Figure.3.17) also reveal that coastal warming event off Tokai happened during this period.

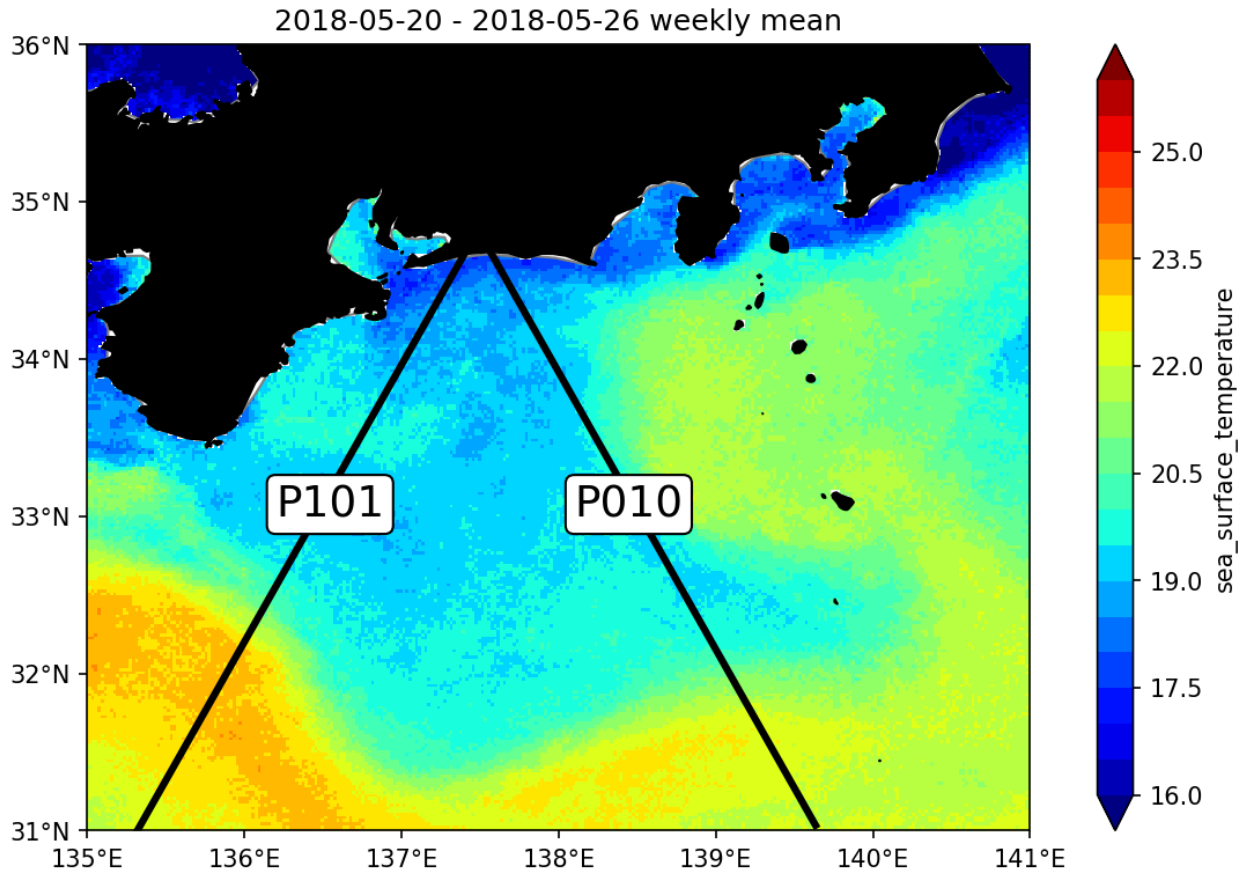

Figure.3.15 Weekly Sea surface temperature (°C) from 2018.05.20 to 2018.05.26

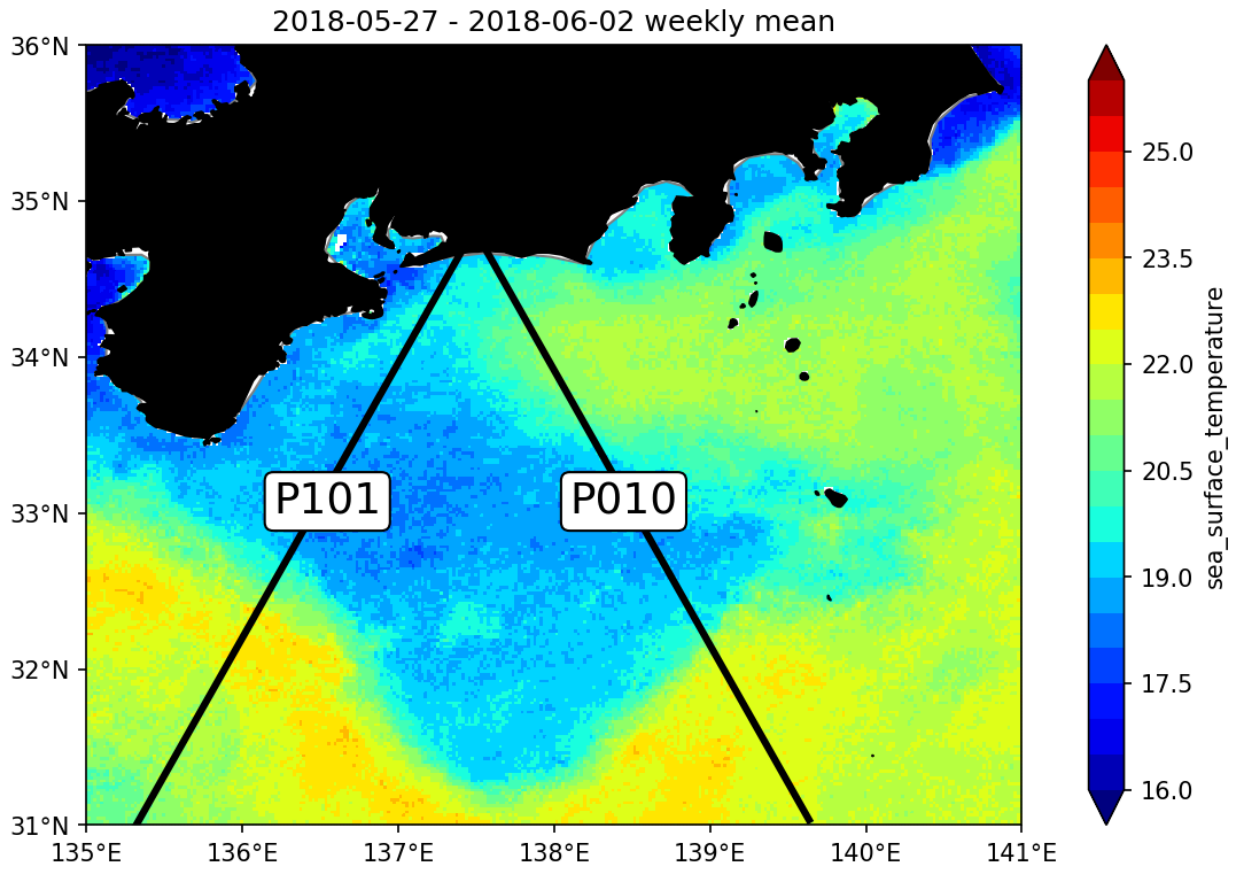

Figure.3.16 Weekly Sea surface temperature (°C) from 2018.05.27 to 2018.06.02

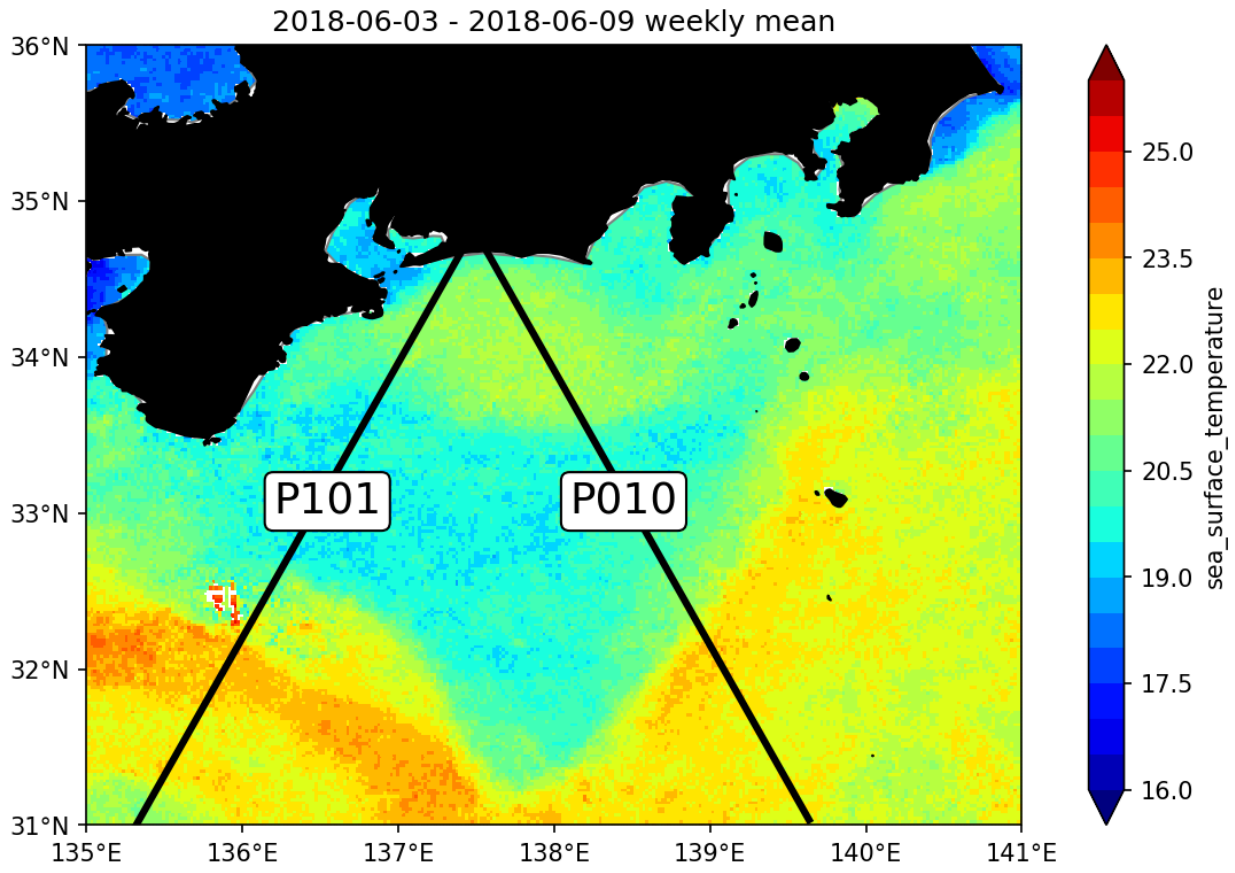

Figure.3.17 Weekly Sea surface temperature (°C) from 2018.06.03 to 2018.06.09

The warm SST moved westward from Pass 010 to Pass 101. We define it as Case II of coastal warming event. Next, we study the SSTAD and SSHAD diagram, to distinguish related signals.

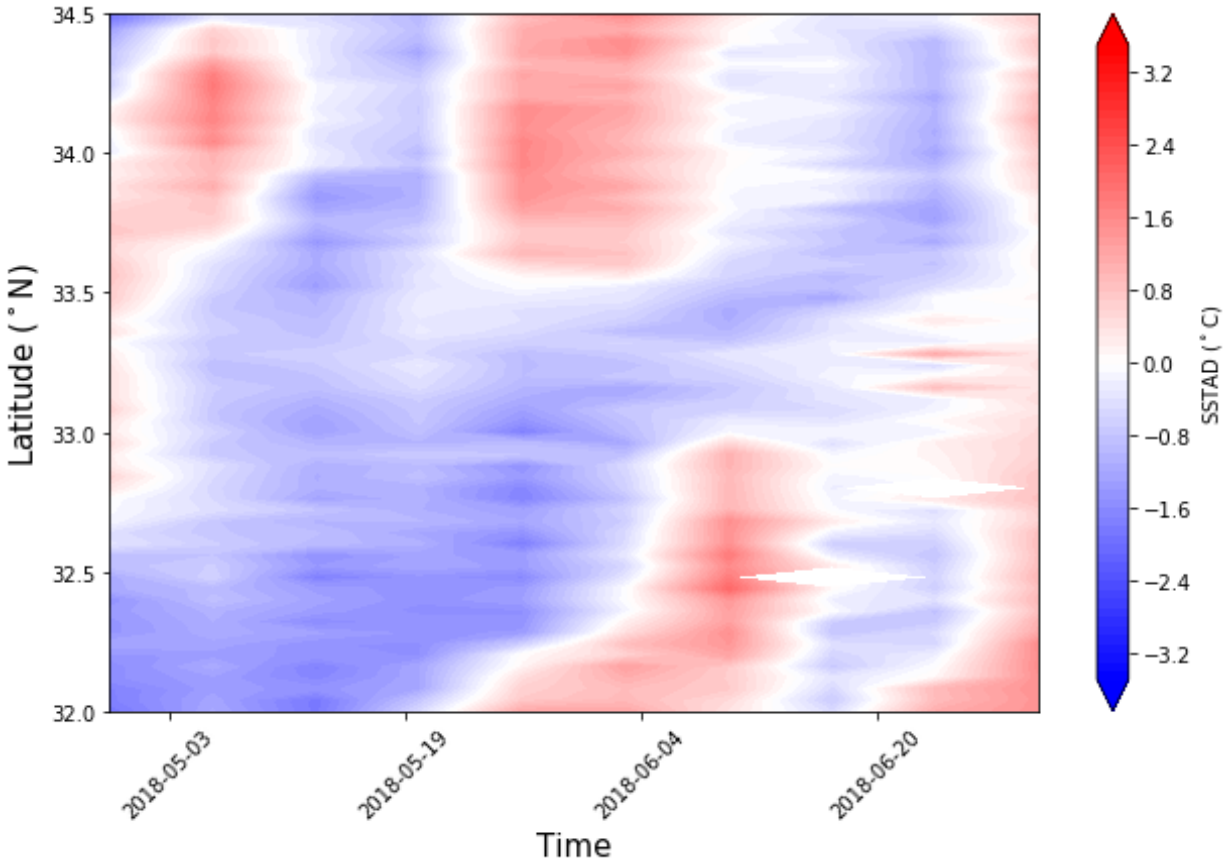

Figure.3.18 Hovmöller diagram of SSTAD along Pass 010 for Case II

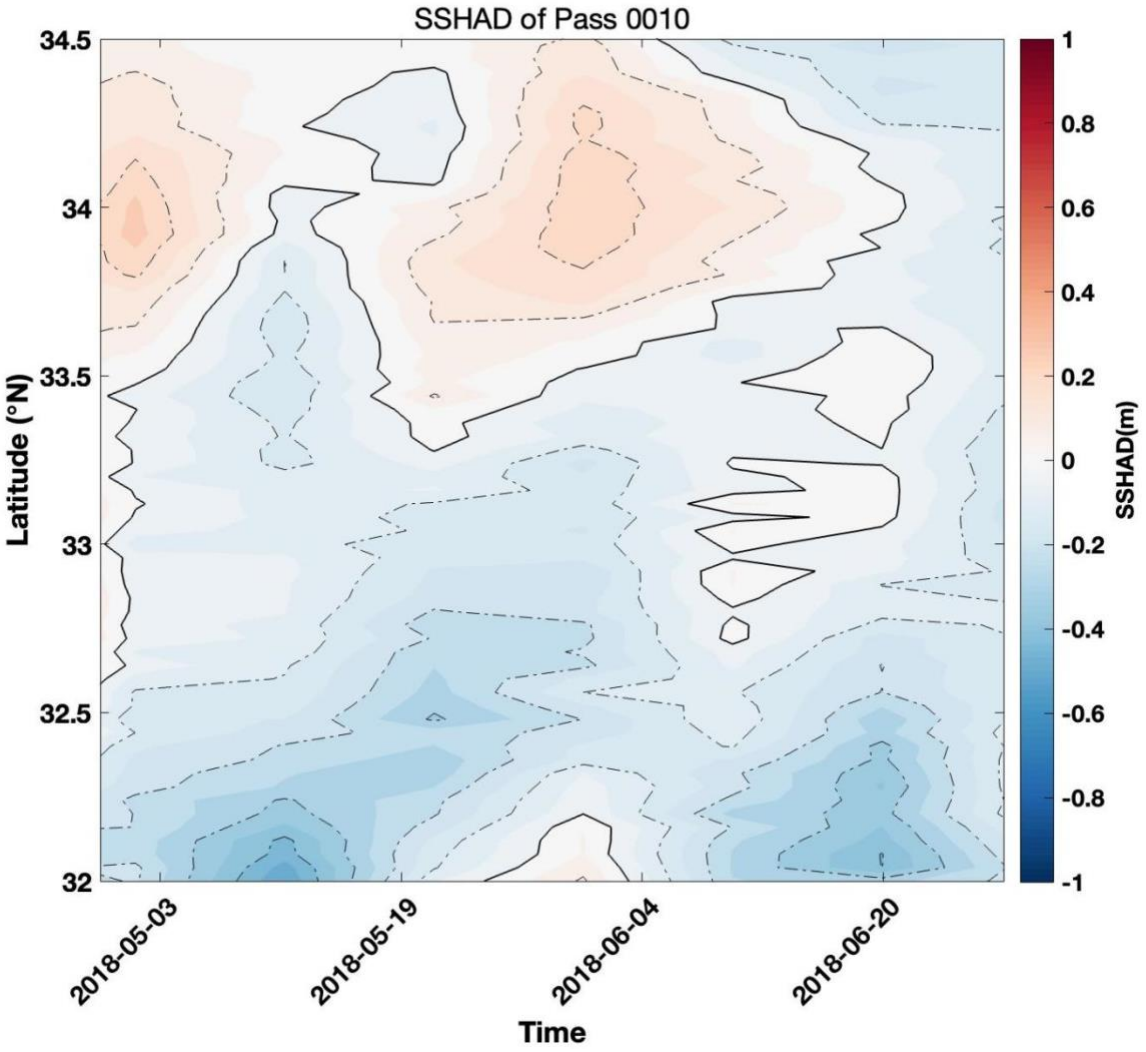

Figure.3.19 Hovmöller diagram of SSHAD along Pass 010 for Case II

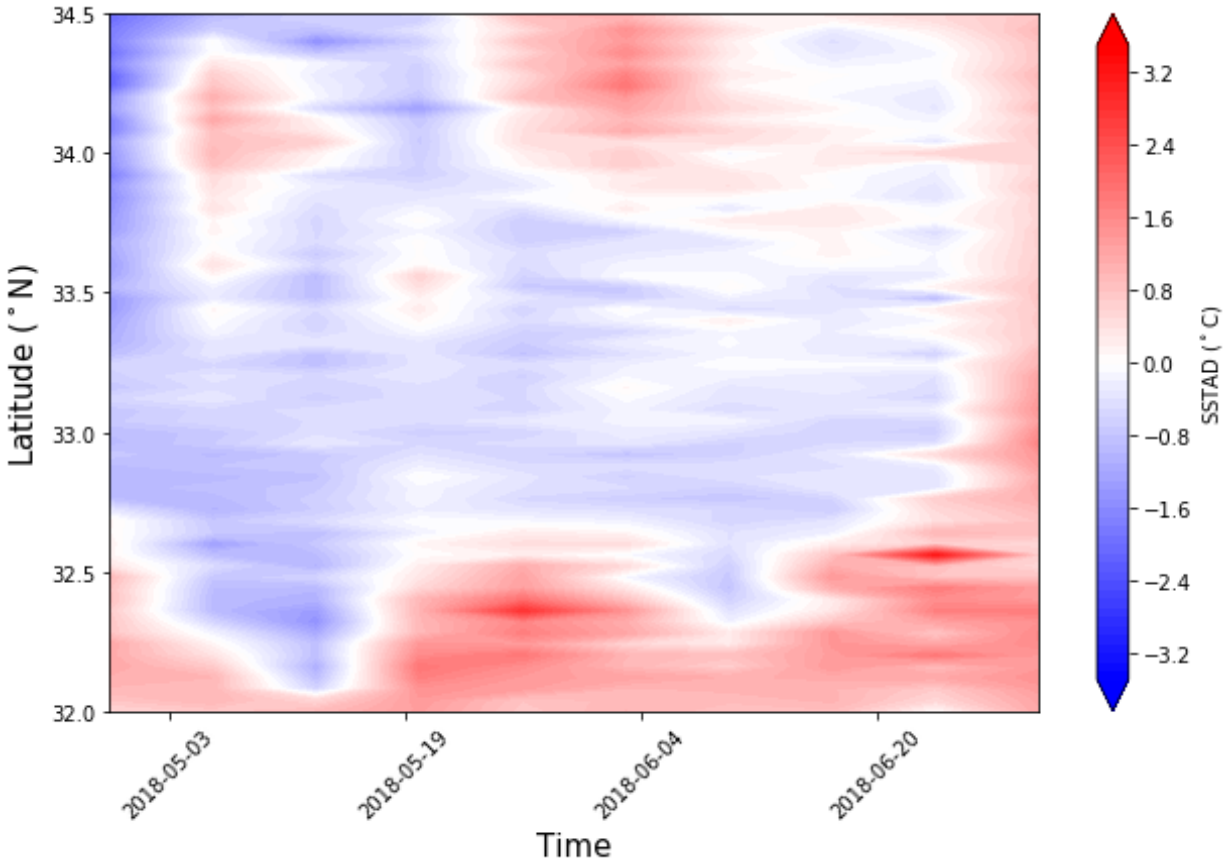

Figure.3.20 Hovmöller diagram of SSTAD along Pass 101 for Case II

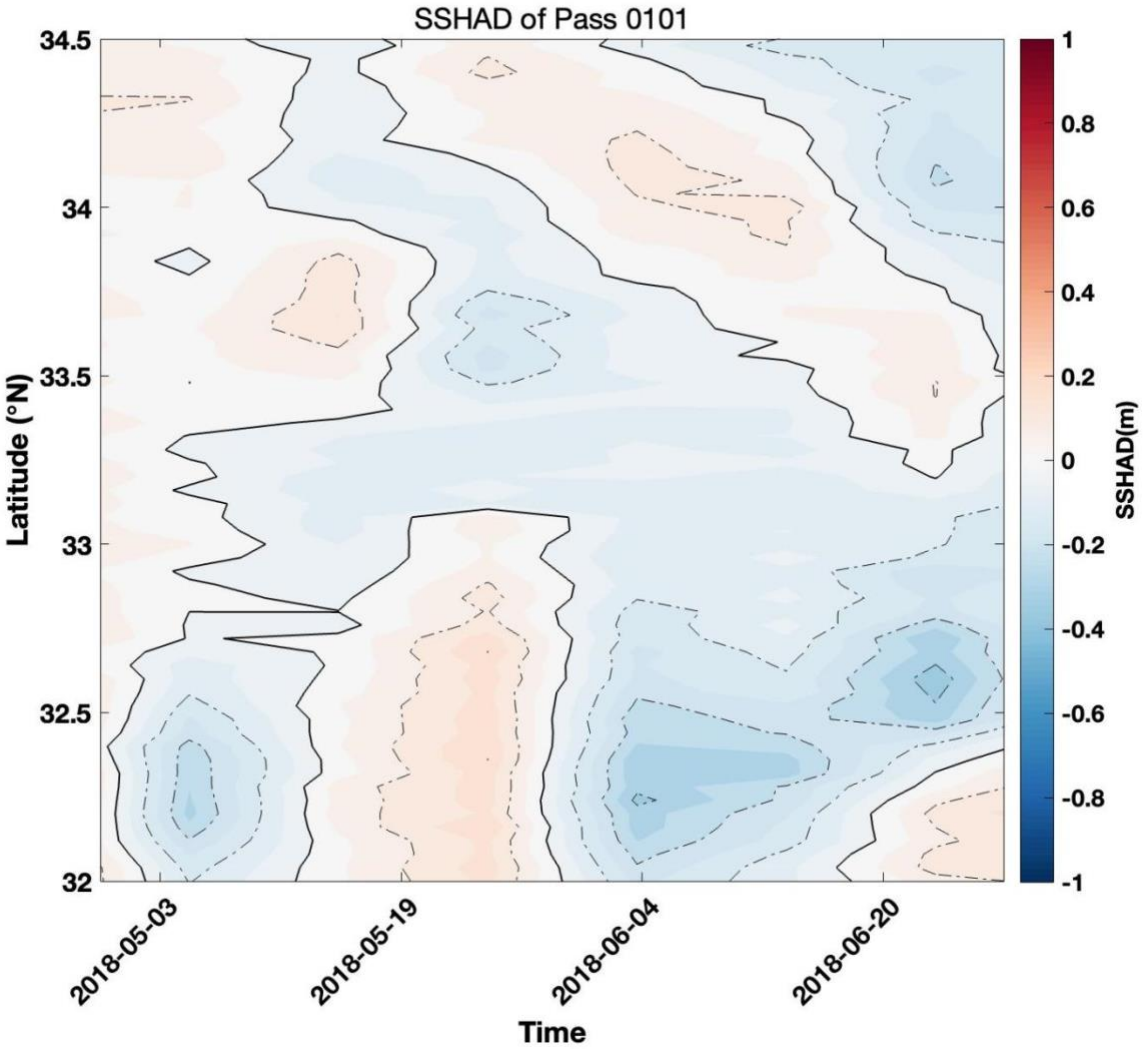

Figure.3.21 Hovmöller diagram of SSHAD along Pass 101 for Case II

The analysis result of Case II is a little different from the Case I. Combining the SST figures, it is reasonable that the variation of Kuroshio axis existed mainly on Pass 101 of [32N, 32.5N]. In SSHAD diagram, the positive value is relatively weak, compared with the SSHAD's value of Pass 010, Case I.

Note that Figure.3.20 and Figure.3.21 show SSTAD and SSHAD are not in phase south of 33N. Appearance of negatives and positives look temporally shifted at 32.25N. These result in low correlation coefficient, which is shown in scatterplot in the next charpter.

3.3.2 Scatter Plot

To study more Case II, we also plot the scatter figure so that the result can be studied quantitatively. As shown in Figure.3.22-Figure.3.23, it shows statistical relationship among the SSTAD and SSHAD. In the figures, statistically insignificant values at 95% confidence level are also not shown.

From Figure.3.22, for Pass 010, we also divide the area mainly into 2 parts:

1) The slope between 32°N and 33.5°N, with large k of 0.105.
2) The slope between 33.5°N and 34.5°N with large k of 0.109.
   For the area between 33.5°N -34.5°N, SSTAD and SSHAD are strongly correlated, and the related signal could be found both in SSTAD field and SSHAD field.

And for the area between 32°N-33.5°N, the large k (0.105) indicates that SSHAD varies largely with the change of SSTAD.

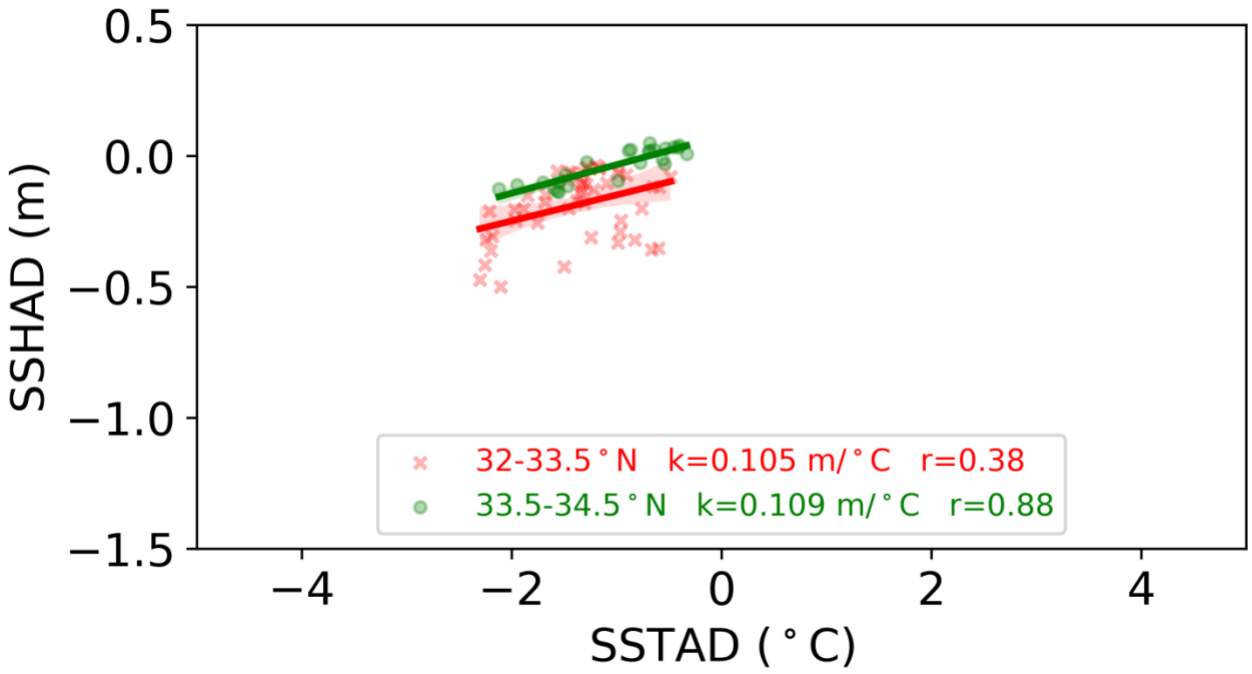

Figure.3.22 Scatter diagram of SSHAD (m) and SSTAD (°C) along Pass 010. Color represents the latitude

For Pass 101, we focus on the area from 32°N to 34.5°N.

From Figure.3.23, for Pass 101, we mainly divide the area into 2 parts,except for the low correlation coefficient of [32.5°N, 33.5°N]:

1) The slope between 32°N and 32.5°N, with the largest k value of 0.126
2) The slope between 33.5°N and 34.5°N, with the small k value of 0.040. This area includes the coastal warming events.

For the area 32°N-32.5°N, the SSHAD and SSTAD of scatter points in Figure.3.23 have a positive correlation relationship. Combing the SST figures, the reason account for the largest k could be the frequent movement of Kuroshio axis along Pass 101 during Case II period.

For the area 33.5°N-34.5°N, the SSHAD and SSTAD of scatter points show the small k, which indicates the small variation of SSHAD with the change of SSTAD, where coastal warming events happened.

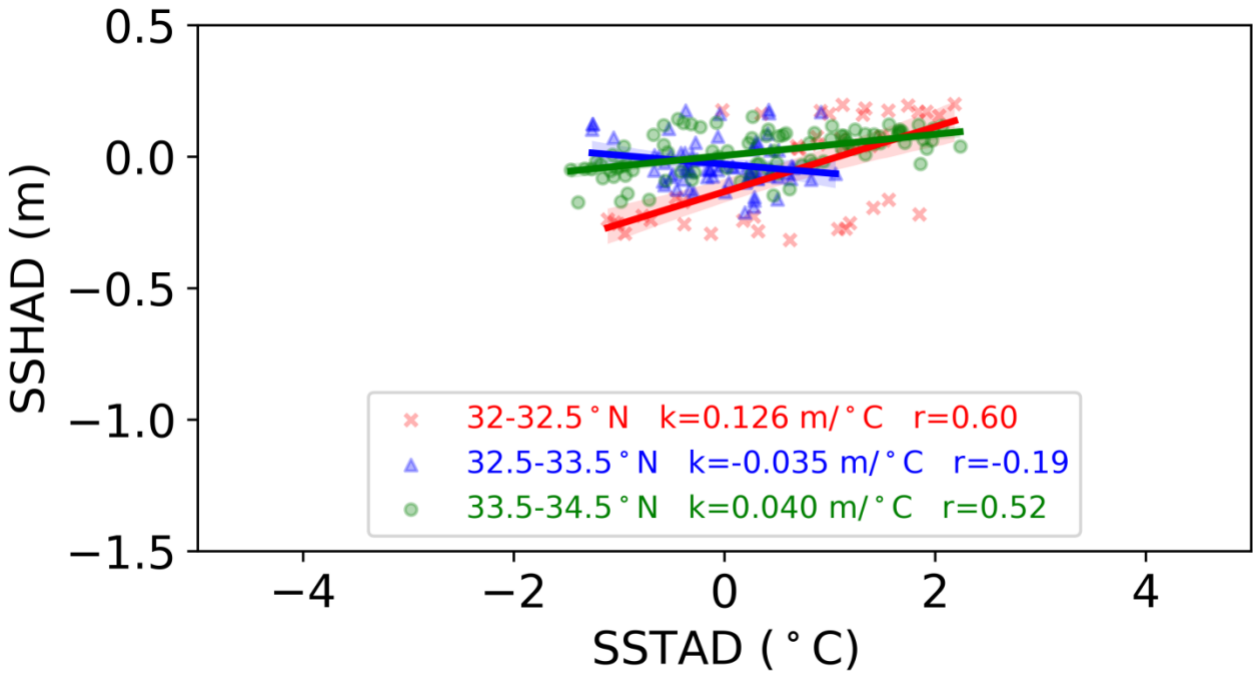

Figure.3.23 Scatter diagram of SSHAD (m) and SSTAD (°C) along Pass 101. Color represents the latitude

To conclude, for Case II of coastal warming event, the reason for the largest k is also the movement of Kuroshio axis during Case II period, and it appeared on Pass 101 (latitude from 32°N to 32.5°N). The small k (0.040 for Pass 101) indicates the small variation of SSHAD with the change of SSTAD, which is related with the coastal warming events.

4. Discussions

Since different k indicates different vertical structure, the slope and further research can be discussed based on the value of k. In Figure.4.1 and Figure.4.2, the small k (below 0.05) indicates that vertical structure of coastal warming events off Tokai is shallow, compared with the Kuroshio itself.

Thermal expansion of seawater plays an important part of sea level rise in the ocean. We consider the coefficient of thermal expansion (c) as a constant :2×10^{-4}/℃, and the seawater column is assumed to expand as Figure.4.3.

In fact, the coefficient of thermal expansion changes with depth, salinity and temperature and cannot be regarded as a constant, which means the temperature increases of water volume are different in every layer. Here, the assumption makes the estimation of equivalent depth much simple.

Since we can calculate the increase in volume from the definition of coefficient of thermal expansion (c). The coefficient of thermal expansion satisfies the following formula:

$$\Delta V = c \times V_0 \times \Delta T,$$

so the $\Delta V/\Delta T = c \times V_0$, and $\Delta V/\Delta T$ is actually the k we calculated before.

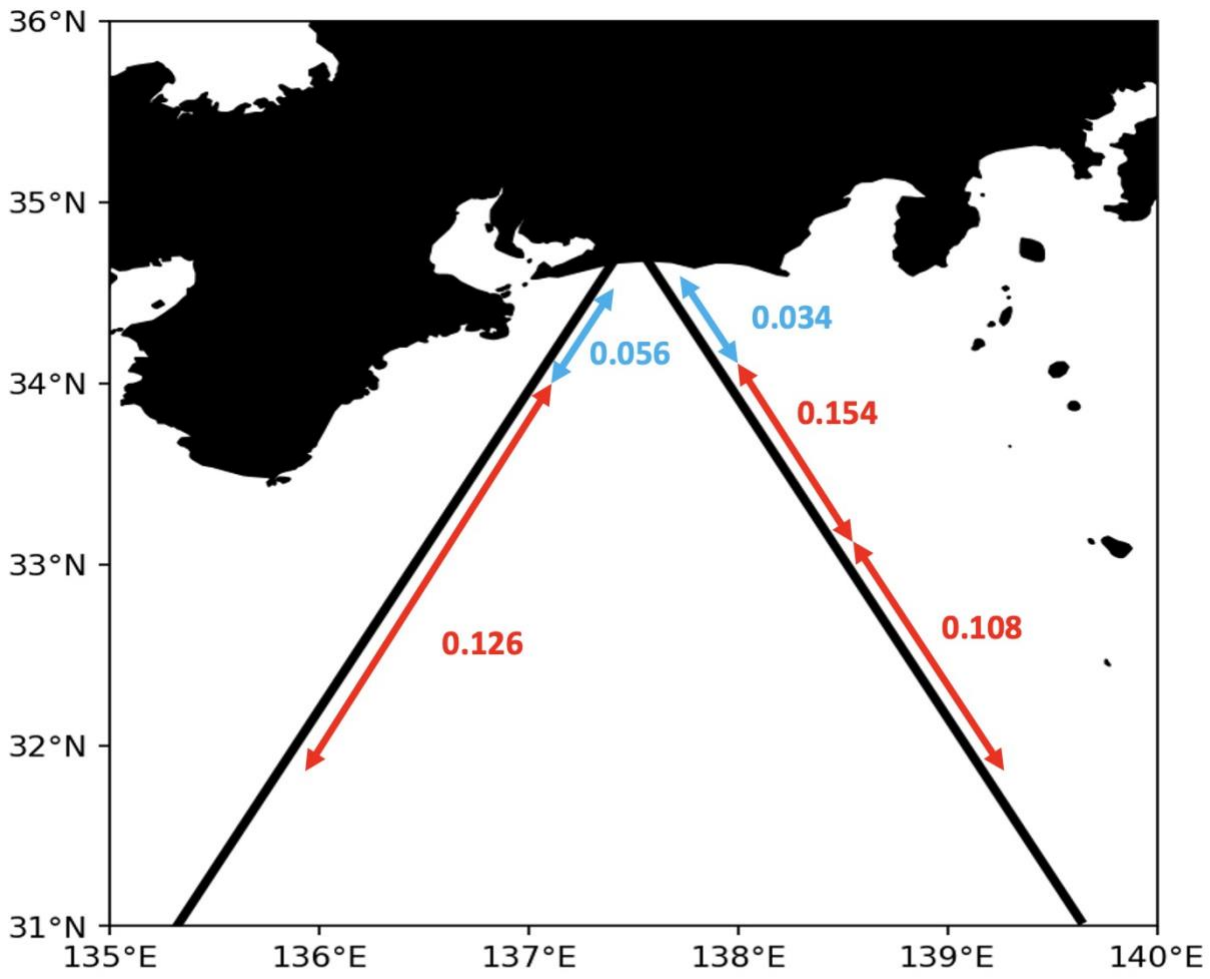

Figure.4.1 Distribution of k value during Case I period

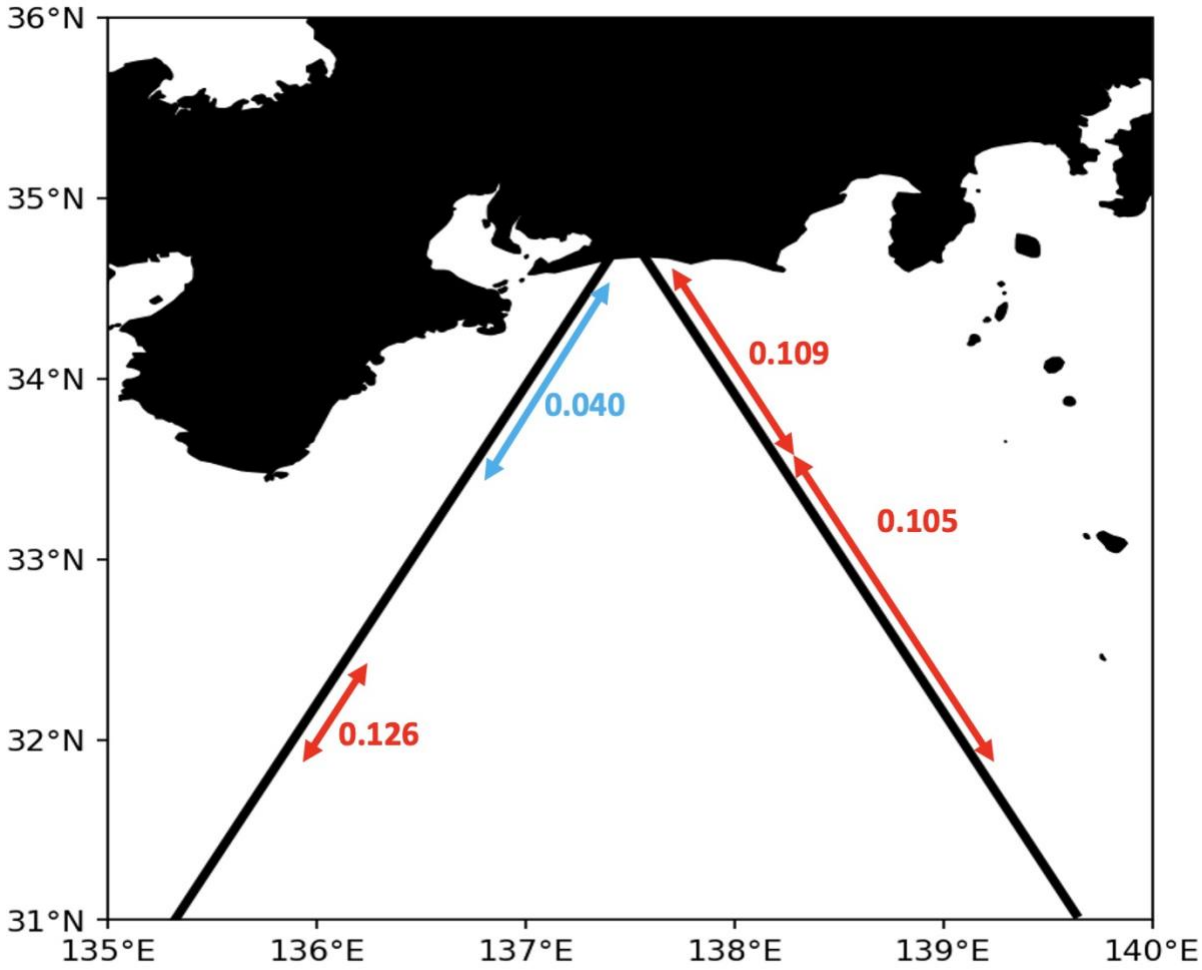

Figure.4.2 Distribution of k value during Case II period

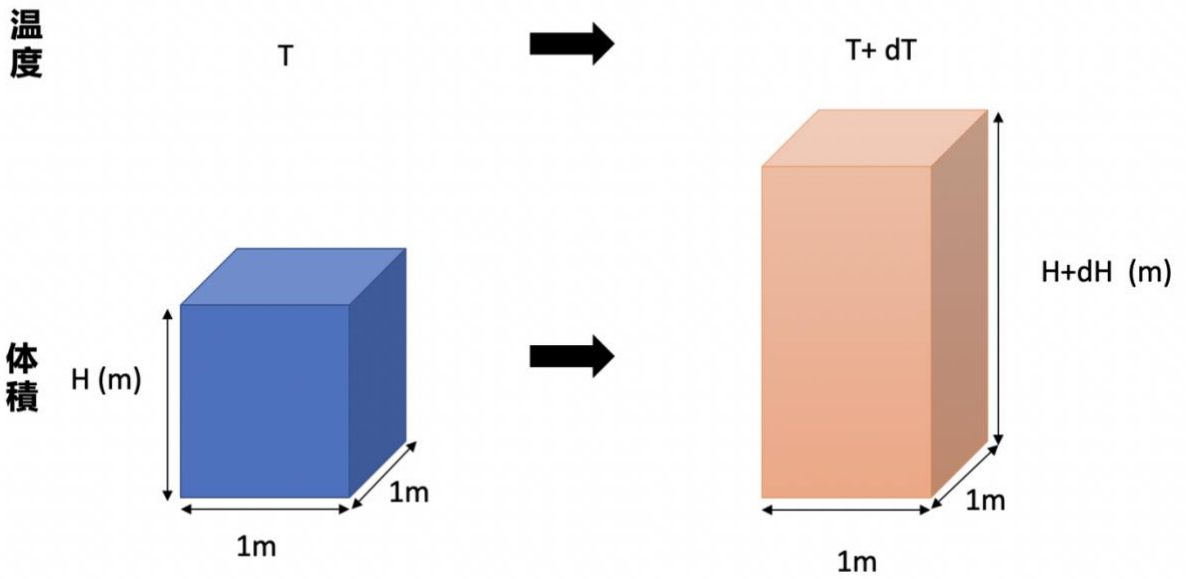

Figure.4.3 Schematic figure of volume expansion of seawater column

This means that the equivalent depth can be estimated by following formula:
H=k/c

The estimated H for Kuroshio current of our study period is around 500-700m, which is reasonable. The estimated H for coastal warming events of Case I and Case II are around 170 m and 200m, respectively. It is possible that thin coastal warming events are caused by pinched-off surface water, which could be separated from the meandering of Kuroshio and moved westward.

Equivalent depth refers to the rough estimation of minimum depth structure. In fact, the real depth of vertical structure is deeper than it.

5. Summary and Conclusions

In this study, the summary of main job is listed as follows:

1. The Himawari gridded SST data is processed and interpolated into SSTAD Hovmöller diagrams, by choosing the LM period reference and suitable reference area.

2. The along-track SSH data is processed and calculated as SSHAD Hovmöller diagrams, to further know the variation of SSH during Case I and Case II period.

3. The statistical relationship (correlation relationship, regression relationship) between SST and SSH during Case I and Case II is studied, by plotting the scatterplots.

4. As comparison, the result of SSTAD and SSHAD when using long-term reference is calculated, and the SSHAD only based on AVISO gridded data is calculated, to better know the difference by using different duration of reference and dataset.

To conclude:

The gridded SSH, SST data and along-track SSH data are processed and analyzed to investigate the coastal warming events during LM period off Tokai district.

And we obtained the following results:

1.Coastal warming events off Tokai during LM period are frequently found, which would influence the SST and SSH in research area.

2.Compared with the Kuroshio itself, coastal warming events in our study have relatively shallow vertical structure.

3.According to the simple estimation from coefficient of thermal expansion, the estimated equivalent depth for coastal warming events is around 170m to 200m.

To further investigate possible reason for coastal warming events, it is necessary to investigate more information to estimate the velocity (like drifting buoys) around research area ,and more cases of coastal warming events should be studied, to better expain the mechanism.

6. References

Banzon, V., Smith, T. M., Steele, M., Huang, B., & Zhang, H.-M. (2020). Improved estimation of Proxy sea surface temperature in the Arctic. Journal of Atmospheric and Oceanic Technology, 37(2), 341–349. https://doi.org/10.1175/JTECH-D-19-0177.1

Bessho, K., Date, K., Hayashi, M., Ikeda, A., Imai, T., Inoue, H.,Kumagai, Y., Miyakawa, T., Murata, H., Ohno, T., Okuyama, A., Oyama, R., Sasaki, Y., Shimazu, Y., Shimoji, K., Sumida, Y., Suzuki, M., Taniguchi, H., Tsuchiyama, H., … Yoshida, R. (2016). An Introduction to Himawari-8/9& mdash; Japan& rsquo; s New-Generation Geostationary Meteorological Satellites. Journal of the Meteorological Society of Japan. Ser. II, 94(2), 151–183. https://doi.org/10.2151/jmsj.2016-009

Dibarboure G., M-I. Pujol, F. Briol, P.-Y. Le Traon, G. Lanichol, N. Picot, F. Mertz, P. Escudier, M. Ablain, and C. Dufau: Jason-2 in DUACS: first tandem results and impact on processing and products, Mar.Geod., OSTM Jason-2 Calibration/Validation Special Edition – Part 2, (34), 214-241, doi:10.1080/01490419.2011.584826, 2011

Huang, B., Liu, C., Banzon, V., Freeman, E., Graham, G., Hankins, B., et al. (2021). Improvements of the daily optimum interpolation sea surface temperature (DOISST) version 2.1. Journal of Climate, 34(8), 2923–2939. https://doi.org/10.1175/JCLI-D-20-0166.1

Ichikawa, K. (2019). Remote Sensing of the Kuroshio Current System. In: Barale, V., Gade, M. (eds) Remote Sensing of the Asian Seas. Springer, Cham. https://doi.org/10.1007/978-3-319-94067-0_11

Kawabe, M. (1985) Sea level variations at the Izu Islands and typical stable paths of the Kuroshio. J. Oceanogr. Soc. Japan, 41, 307–326.

Kawabe, M. (1995) Variations of current path, velocity, and volume transport of the Kuroshio in relation with the large meander. J. Phys. Oceanography, 25, 3103–3117

Passaro, M., L. Fenoglio-Marc, and P. Cipollini (2015), Validation of significant wave height from improved satellite altimetry in the German Bight, IEEE Trans. Geosci. Remote Sens., 53(4), 2146– 2156, doi:10.1109/TGRS.2014.2356331.

Pujol, M.-I., Faugère, Y., Taburet, G., Dupuy, S., Pelloquin, C., Ablain, M., and Picot, N.: DUACS DT2014: the new multi-mission altimeter data set reprocessed over 20 years, Ocean Sci., 12, 1067-1090, doi:10.5194/os-12-1067-2016, 2016

Sugimoto, S., Qiu, B., & Kojima, A. (2020). Marked coastal warming off Tokai attributable to Kuroshio large meander. Journal of Oceanography, 76(2), 141-154. https://doi.org/10.1007/s10872-019-00531-8

Sugimoto, S., Qiu, B., & Schneider, N. (2021). Local atmospheric response to the Kuroshio large meander path in summer and its remote influence on the climate of Japan. Journal of Climate, 34(9), 3571-3589.

https://doi.org/10.1175/JCLI-D-20-0387.1

Usui, N., Tsujino, H., Nakano, H., Fujii, Y., Kamachi, M. (2011) Decay mechanism of the 2004/05 Kuroshio large meander. J Geophys Res 116:C10010. https ://doi.org/10.1029/2011J C007009

Zhang, Z., Ichikawa, K. Influence of the Kuroshio Fluctuations on Sea Level Variations along the South Coast of Japan. J Oceanogr 61, 979–985 (2005). https://doi.org/10.1007/s10872-006-0014-1

7.Acknowledgement

Over the course of my researching and writing this master thesis, I received a lot of support and guidance. So here, in this chapter, I want to give my heartfelt thanks to the person who have ever helped me in this amazing journey.

First, I am extremely grateful to my supervisor, Kaoru Ichikawa, the Associate Professor from the Research Institute for Applied Mechanics of Kyushu University. During the period of master study, it is my honor to benefit from his valuable advice. Those video recordings and detailed introduction through email helped me a lot. Every time I feel disappointed with my research, I would like to see these materials. Furthermore, I was always inspired by his serious attitude towards research and work. Thank you for all the motivation, inspiration from the bottom of my heart.

Second, I want to express my appreciation to my predecessor, Fu Yue, who always keep communication with me. We communicated study progress and theis progress all the time.

Finally, I am grateful for the support from my parents and myself. It’s an amazing journey. Although with bad body condition for most of the master time, I didn’t give up. In the future, I will keep working hard and stay humble.

Appendix

A.1 Results based on the long-term reference

At before, the LM reference (2017.09-2019.04) is used to calculate the SSTAD and SSHAD. The purpose is to better describe coastal warming events, which happened during LM period. To prove the Usefulness of the LM reference, now the Long-term reference (1993.01-2012.12) is additionally used, and the results are listed as follows.

A.1.1 Result of Case study I for coastal warming event

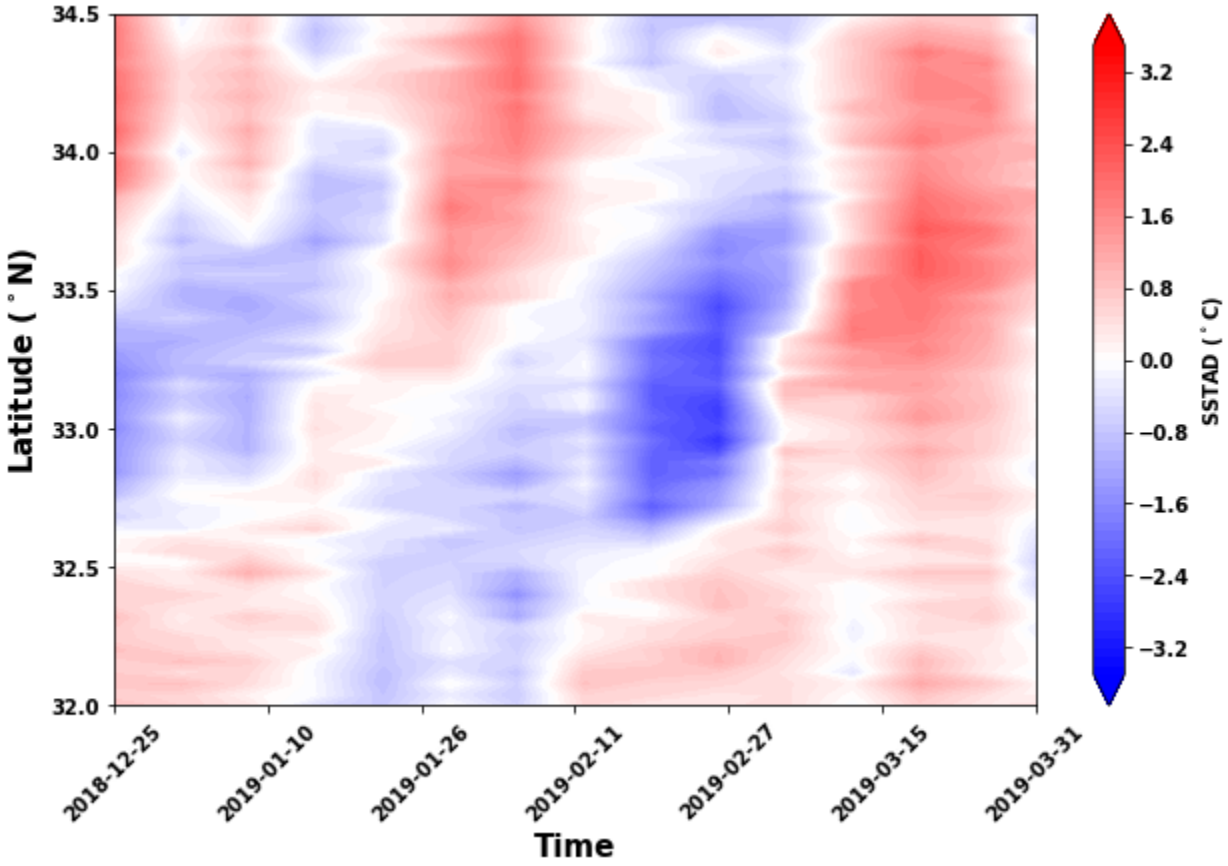

Figure. Hovmöller diagram of SSTAD along Pass 010 for Case I, based on Long-term reference.

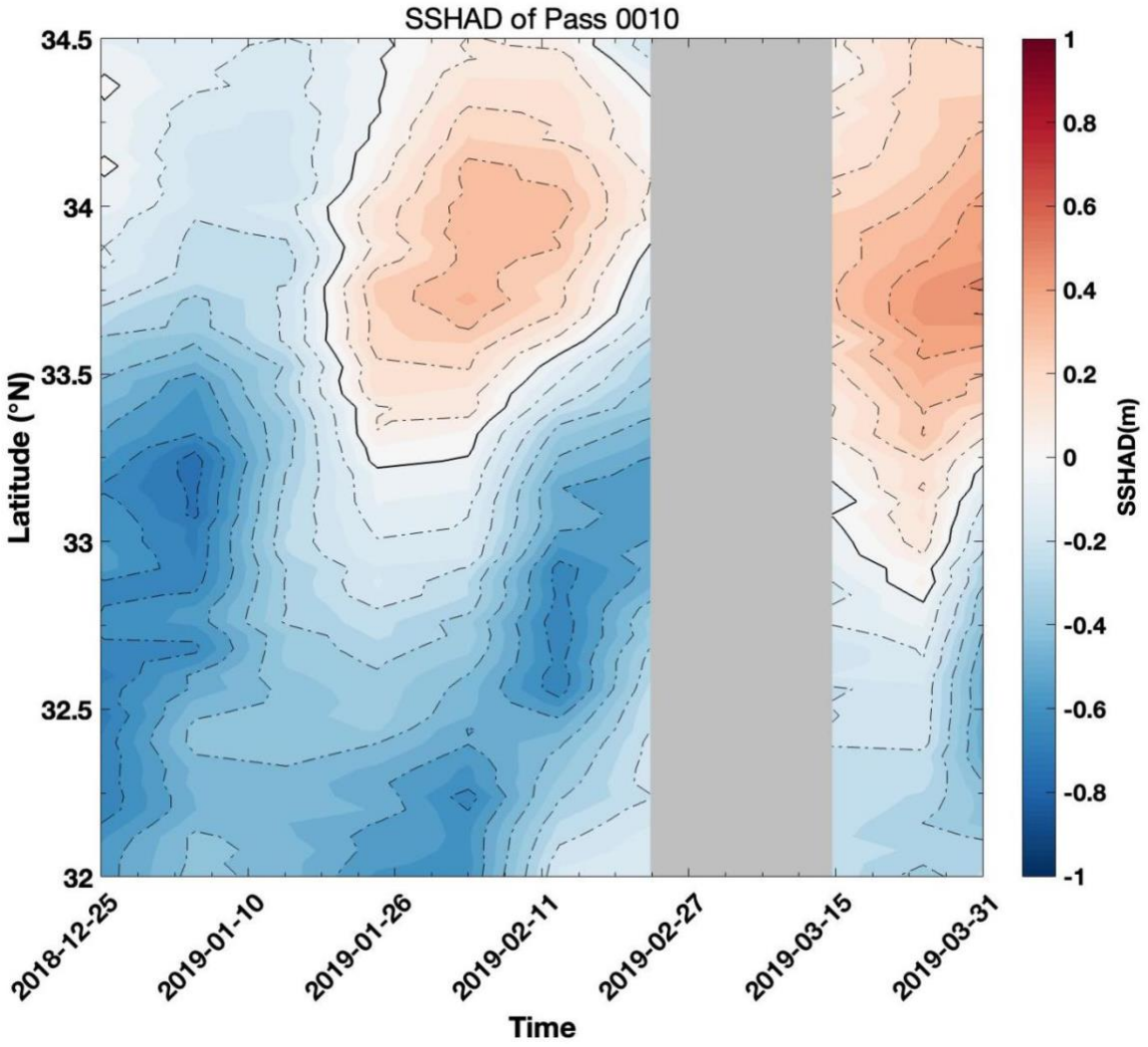

Figure. Hovmöller diagram of SSHAD along Pass 010 for Case I, based on Long-term reference.

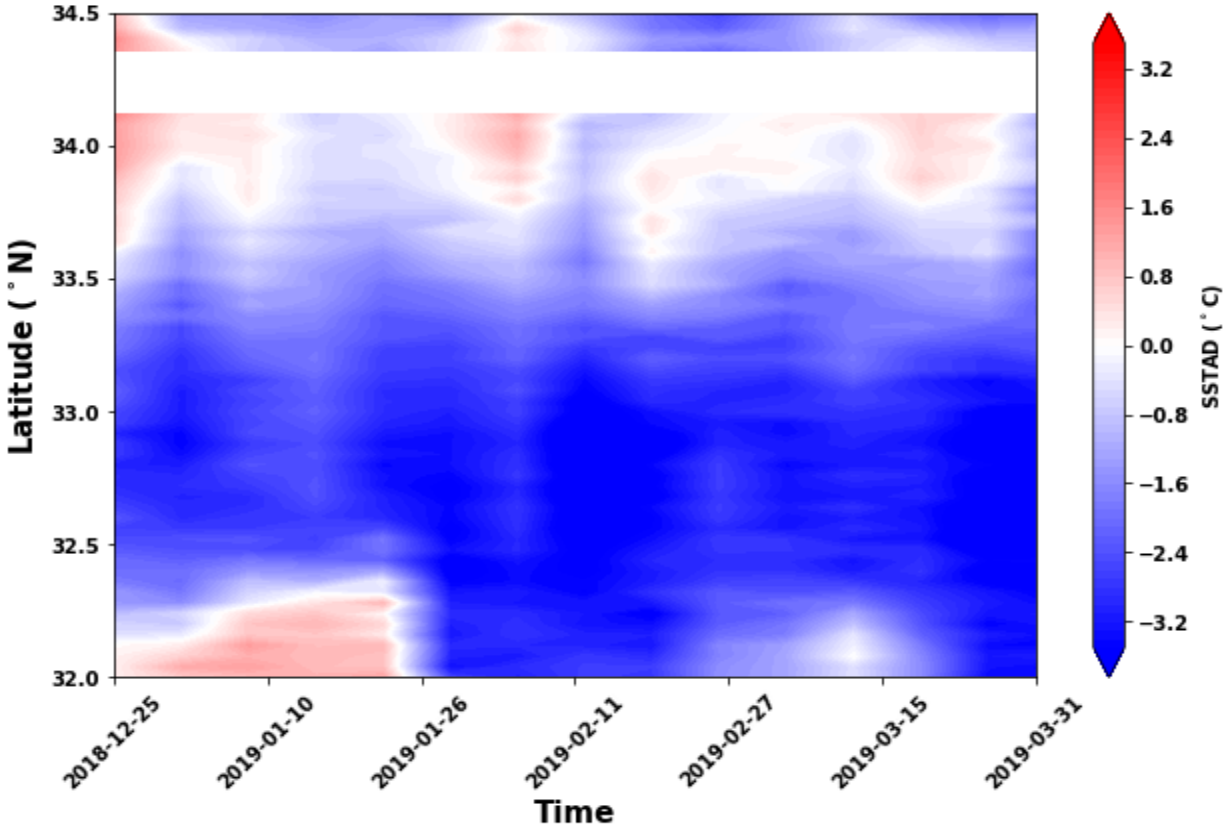

Figure. Hovmöller diagram of SSTAD along Pass 101 for Case I, based on Long-term reference.

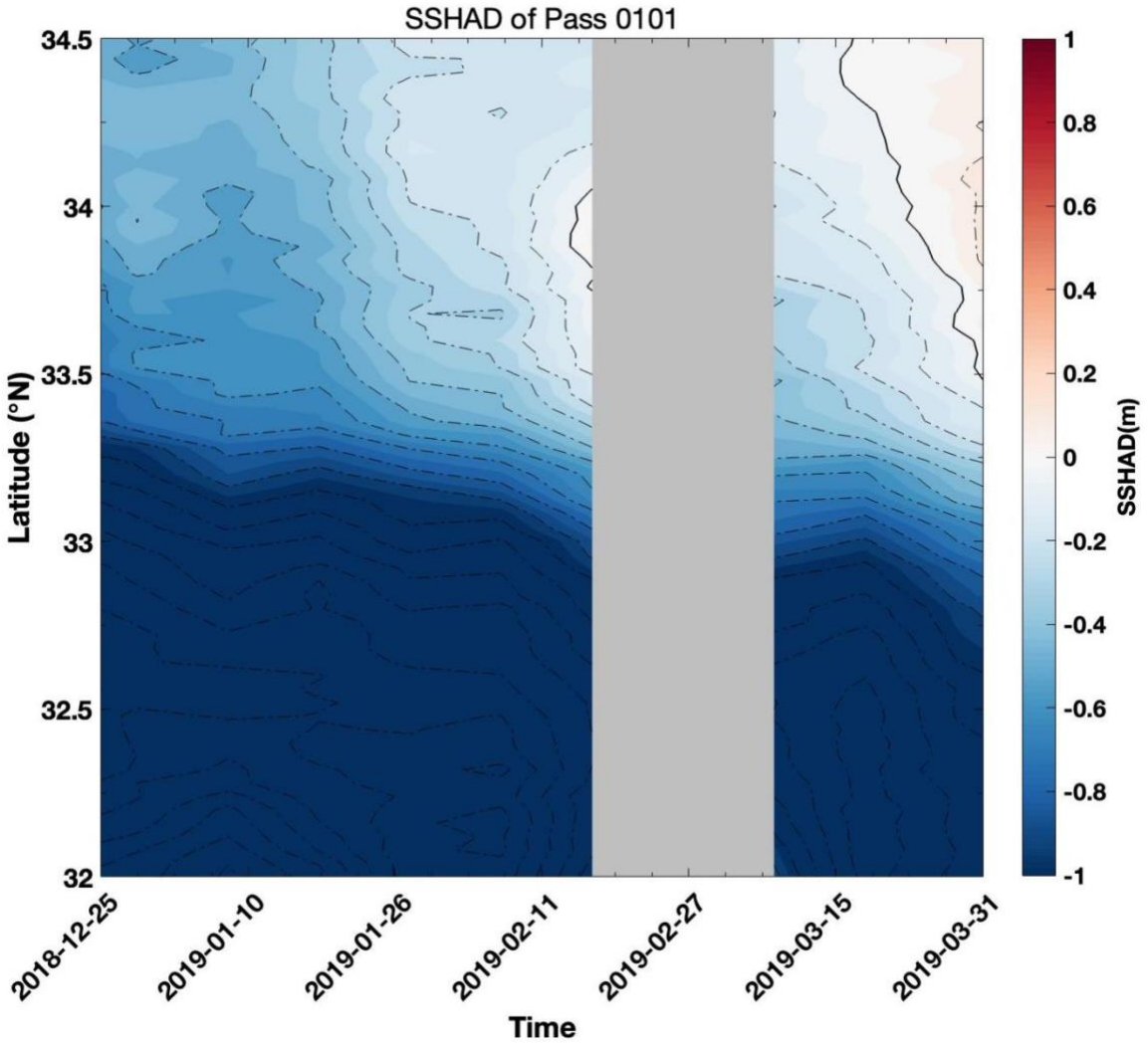

Figure. Hovmöller diagram of SSHAD along Pass 101 for Case I, based on Long-term reference

A.1.2 Result of Case study II for coastal warming event

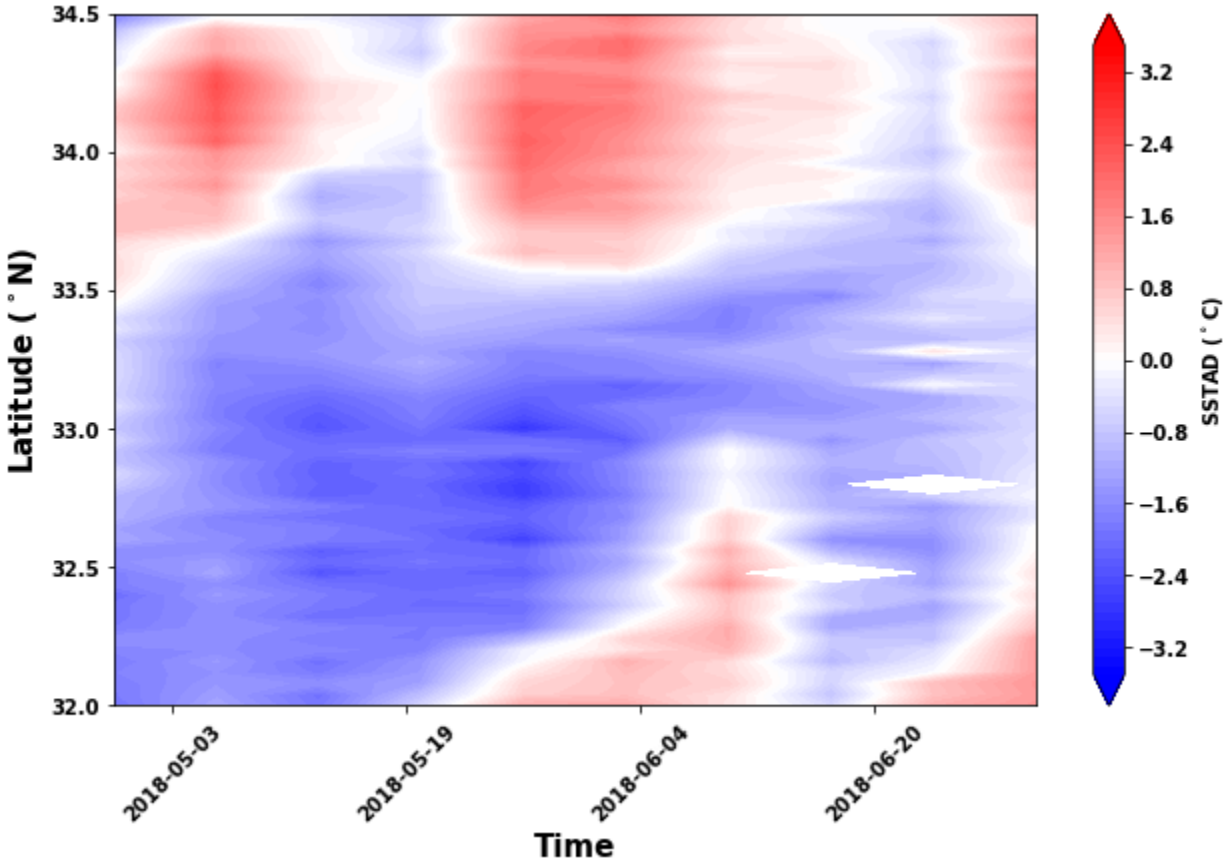

Figure. Hovmöller diagram of SSTAD along Pass 010 for Case II, based on Long-term reference

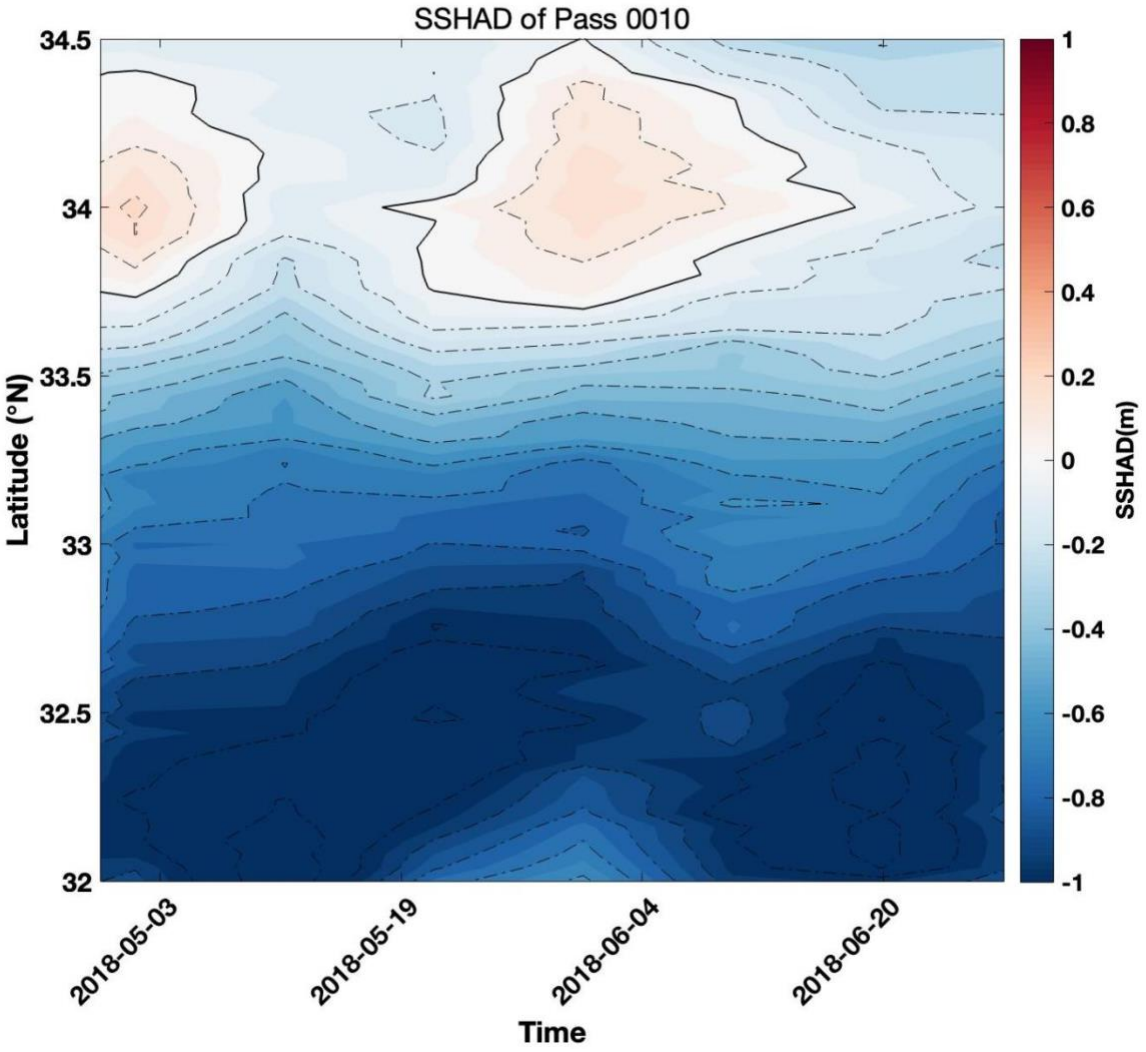

Figure. Hovmöller diagram of SSHAD along Pass 010 for Case II, based on Long-term reference

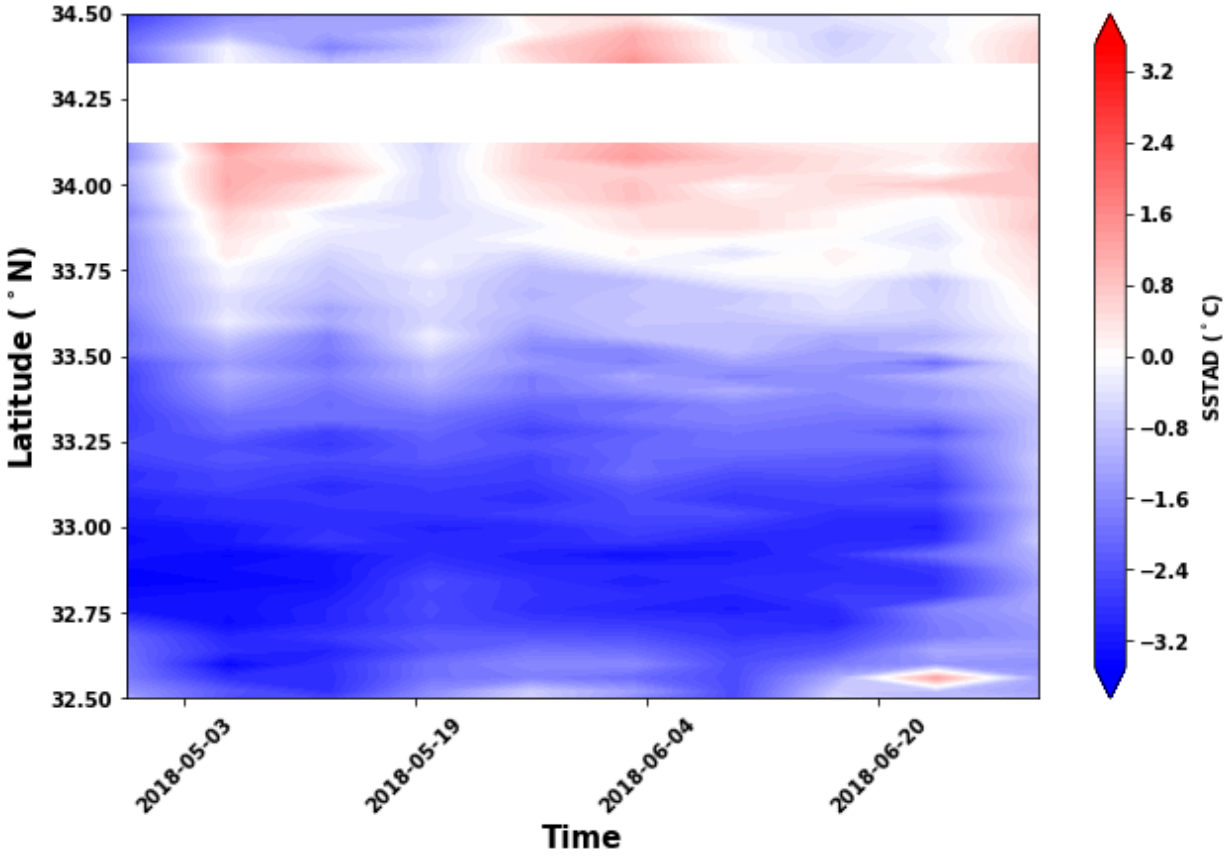

d

Figure. Hovmöller diagram of SSTAD along Pass 101 for Case II, based on Long-term reference

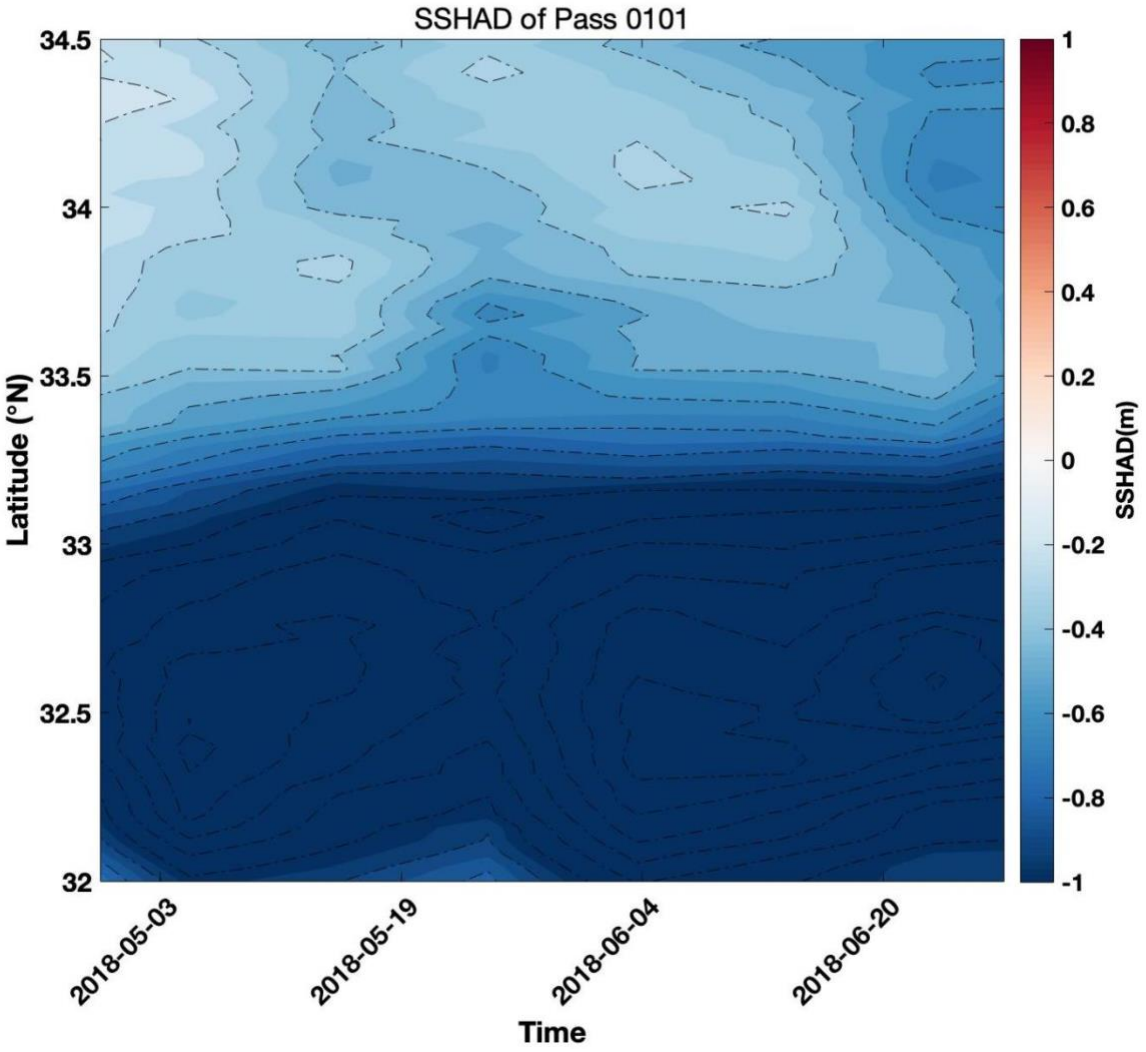

Figure. Hovmöller diagram of SSHAD along Pass 101 for Case II, based on Long-term reference

To conclude, the SSHAD and SSTAD based on long-term reference are not clear to identify characteristics of coastal warming events, compared with the SSHAD and SSTAD based on LM reference. The comparison points out that the choice of LM reference in this study is useful.

A.2 Results of SSHAD when only using AVISO gridded data

A.2.1 For Case I of coastal warming events

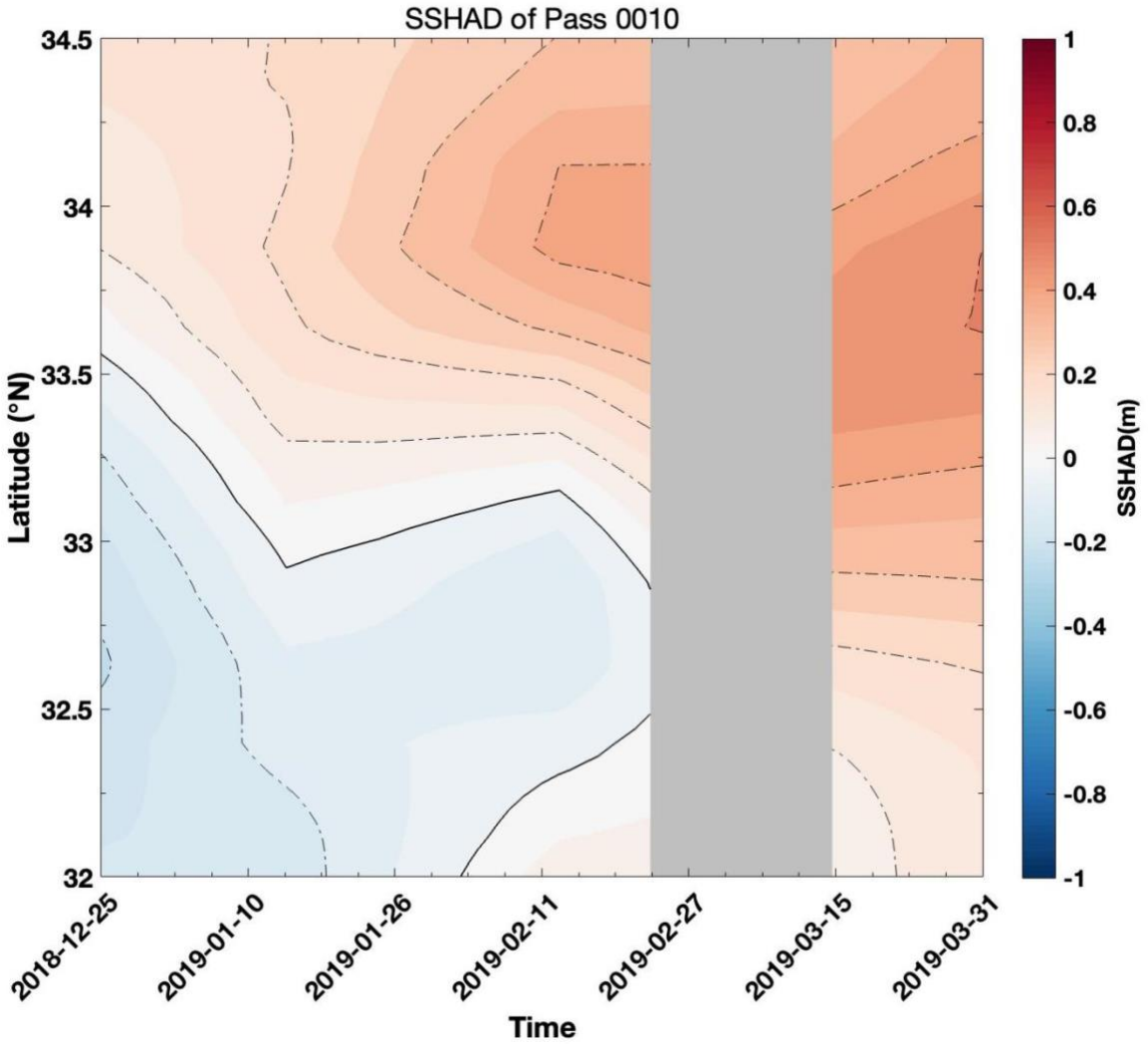

Figure. Hovmöller diagram of SSHAD along Pass 010 for Case I, based on LM reference

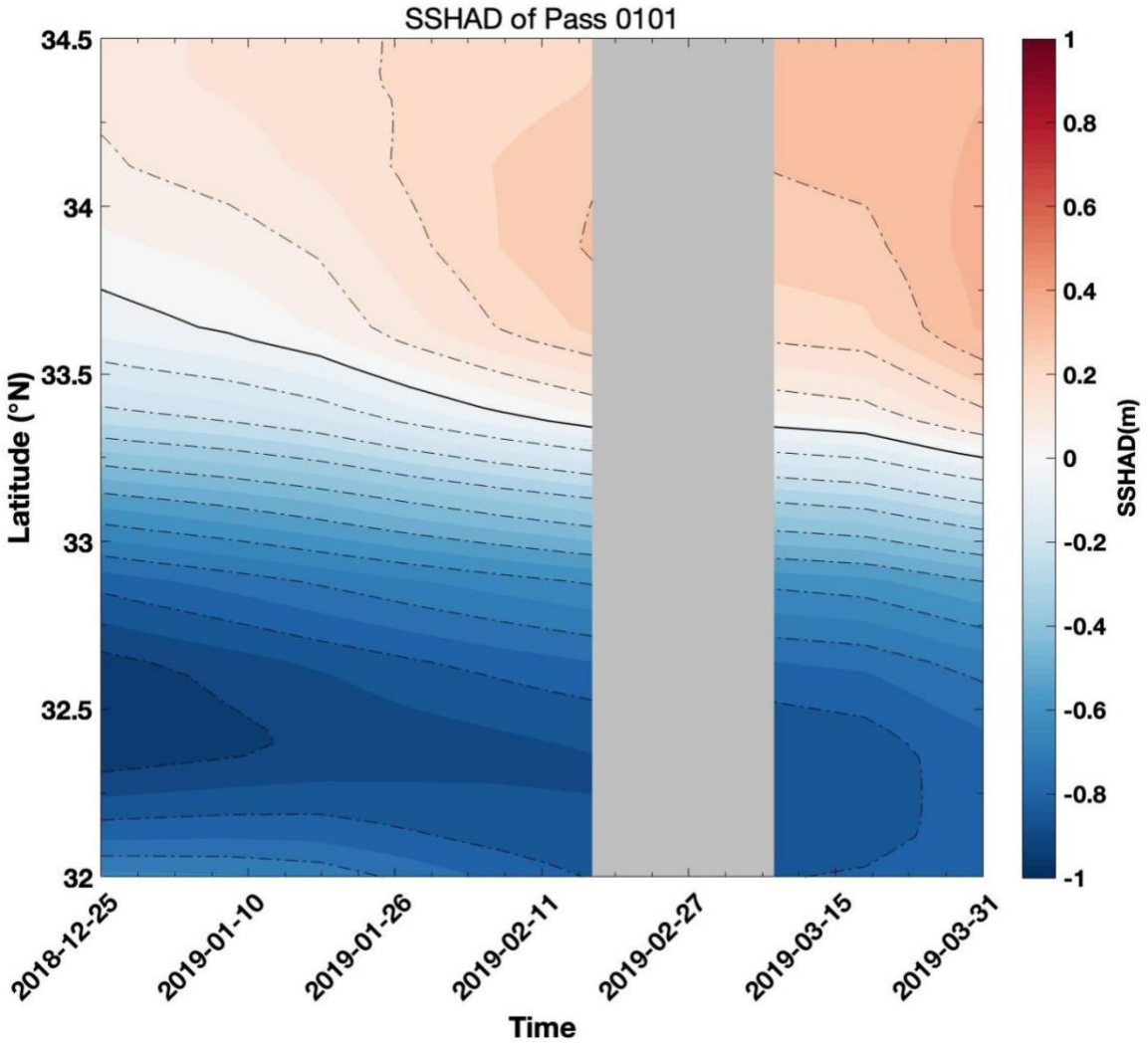

Figure. Hovmöller diagram of SSHAD along Pass 101 for Case I, based on LM reference

A.2.2 For Case II of coastal warming events

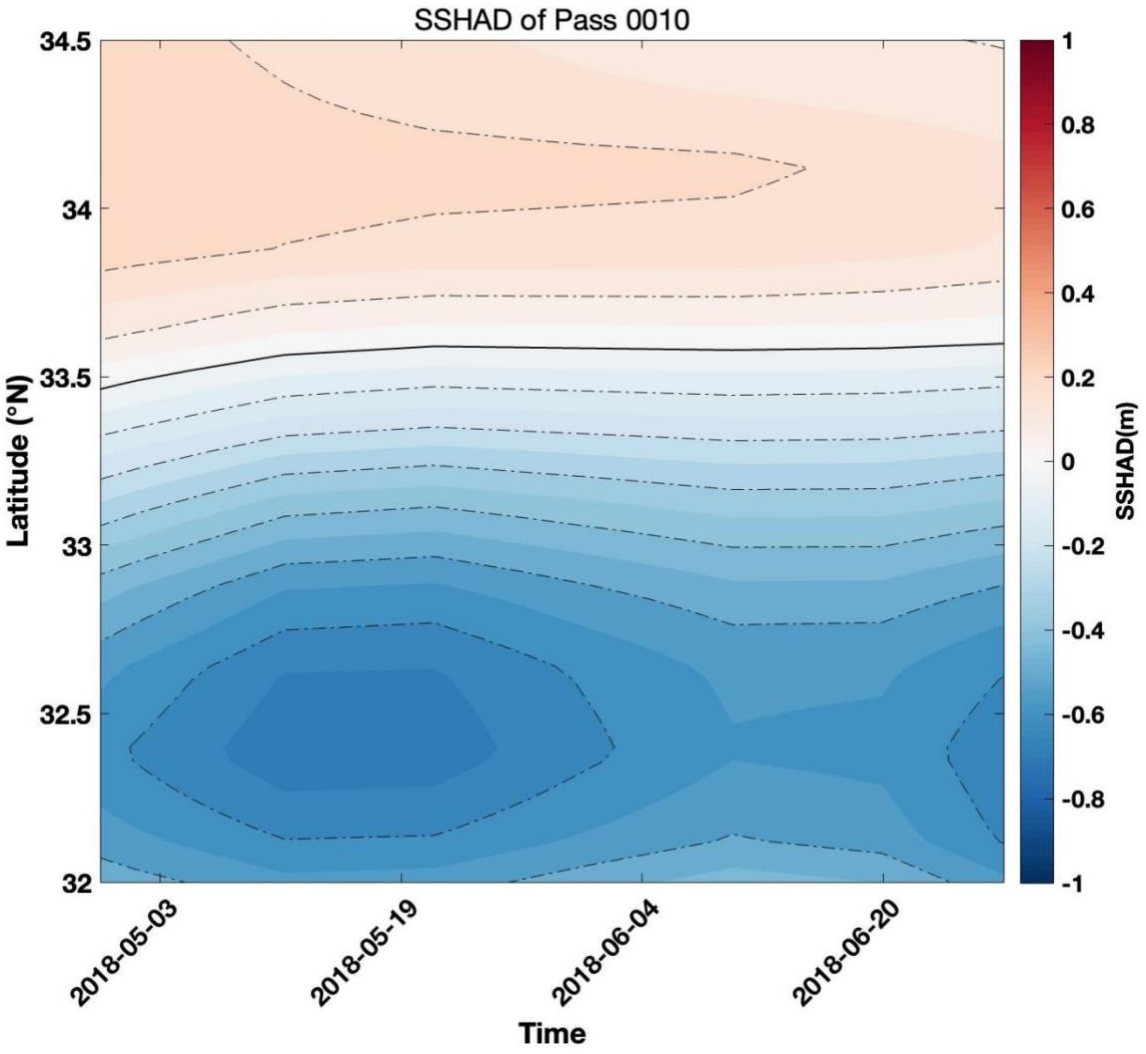

Figure. Hovmöller diagram of SSHAD along Pass 010 for Case II, based on LM reference

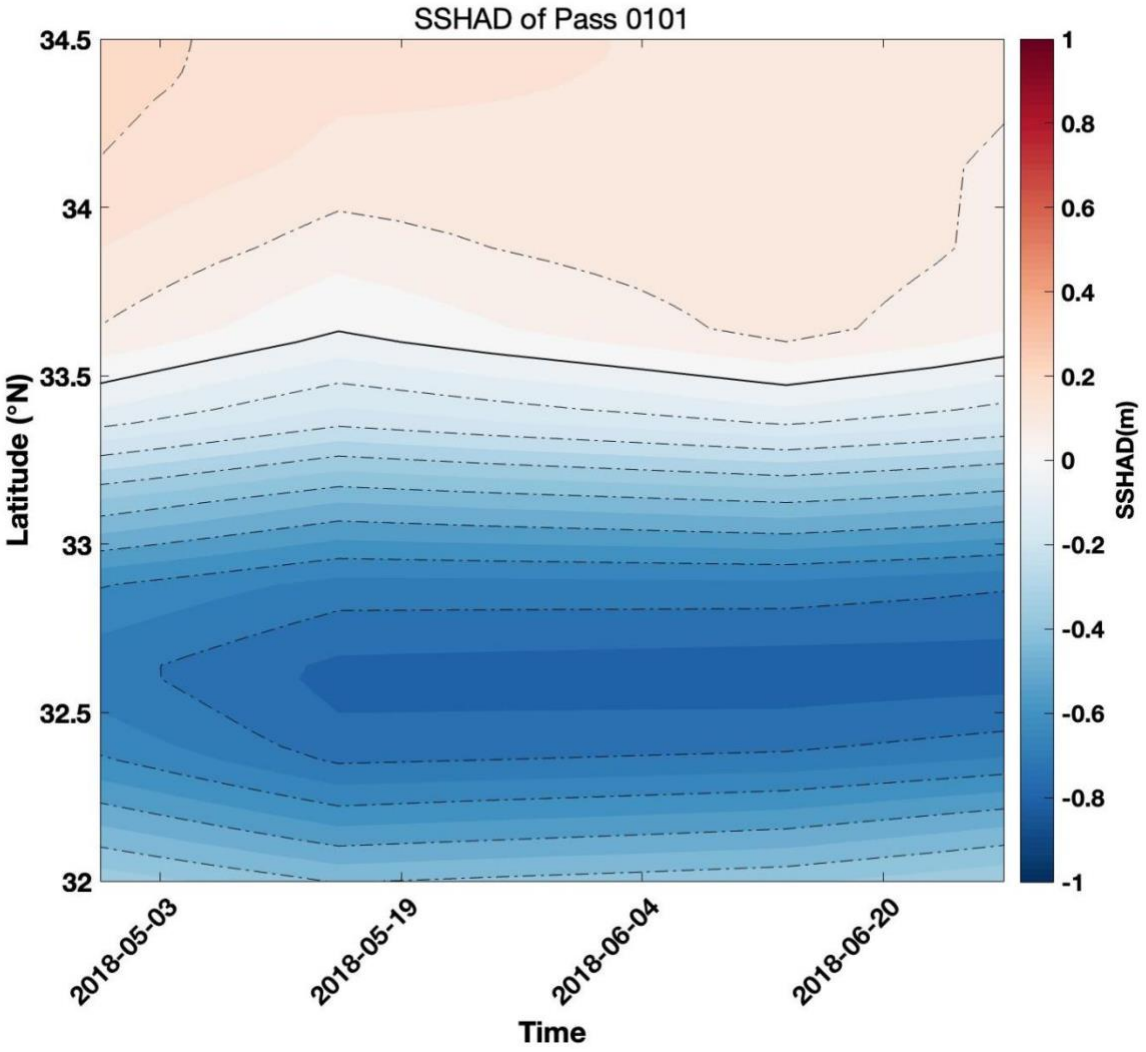

Figure. Hovmöller diagram of SSHAD along Pass 101 for Case II, based on LM reference